Tools for Mapping the Links Between Stimuli, Affective States, and Behavior through Whole-Brain Imaging in Zebrafish Larvae

by

Caroline Lige Zhang

B.S. in Physics and B.A. in Mathematics
Drexel University (2018)
A.M. in Physics
Harvard University (2021)

Submitted to the Program in Media Arts and Sciences, School of Architecture and Planning, in partial fulfillment of the requirements for the degree of
Master of Science
at the
Massachusetts Institute of Technology

May 2024

Authored by: Caroline Lige Zhang
Program in Media Arts and Sciences
May 17, 2024

Certified by: Edward S. Boyden
Professor, Media Arts and Sciences

Accepted by: Joseph Paradiso
Academic Head, Program in Media Arts and Sciences

Tools for Mapping the Links Between Stimuli, Affective States, and Behavior through Whole-Brain Imaging in Zebrafish Larvae

by

Caroline Lige Zhang

Submitted to the Program in Media Arts and Sciences, School of Architecture and Planning, on May 17, 2024 in partial fulfillment of the requirements for the degree of

Master of Science

Abstract

Affective states, often referred to as emotional states, exert substantial influence on behavior and decision-making processes. Traditionally, researchers have turned to functional imaging to delve into the neural mechanisms that drive both behavior and decision making. However, functional imaging of behaving animals often focuses on a singular brain region. Whole-brain imaging, on the other hand, has the capacity to significantly advance our understanding of the brain's functional architecture. In this pursuit, zebrafish larvae emerge as an ideal model for whole-brain imaging due to their transparency, small size, genetic manipulability, rapid development, high reproducibility,

Recent advances in protein engineering and fluorescence microscopy have empowered researchers to observe neural activity across extensive neuronal populations. Genetically Encoded Calcium Indicators (GECIs) and Genetically Encoded Voltage Indicators (GEVIs) provide the means to probe brain dynamics with single-cell precision. The advent of lightsheet microscopy technologies has further enriched our capabilities, enabling the recording of brain activity at remarkable frame rates, ranging from several hundred to several thousand frames per second, all while the animal is exposed to precise visual, auditory, and/or olfactory stimulation. Leveraging these experimental advancements in conjunction with machine learning and computer vision techniques, our study aims to forge connections between stimulation, neural activity, and behavior through a larval zebrafish model.

Thesis Advisor: Edward S. Boyden
Title: Y. Eva Tan Professor in Neurotechnology

Tools for Mapping the Links Between Stimuli, Affective States, and Behavior through Whole-Brain Imaging in Zebrafish Larvae

by

Caroline Zhang

This master thesis has been reviewed and approved by the following committee members

Thesis Advisor:

Edward S. Boyden, Ph.D.
Y. Eva Tan Professor in Neurotechnology, Media Arts and Sciences, MIT

Thesis Reader:

Liam Paniski, Ph.D.
Professor, Department of Statistics and Neuroscience, Columbia University

Thesis Reader:

Yuechuan Lin, Ph.D
Research Scientist, Department of Mechanical Engineering, MIT

TABLE OF CONTENTS

List of Figures:

List of Tables:

Chapter 1: Introduction

The exploration of animal affect states, also known as emotional states, has garnered increased interest within the fields of neuroscience and psychology [1] [2]. Despite concerted efforts by researchers to comprehend the mechanisms underlying these affective states and their subsequent behavioral implications, the intricate processes governing how neuronal interactions give rise to these phenomena remain largely elusive. Our study is centered on elucidating the intricate relationship between stimuli, affective states, behavior, and neural activity at a single-cellular level across the whole brain of a small animal.

To systematically investigate the workings of decision-making, we turn to frameworks like the 'Four Whys' framework (Function, Evolution/Adaptation, Causation/Mechanism and Development) advocated by ethologist Niko Tinbergen[3], and David Marr's[4] three-tiered approach in cognitive science—namely, the computational theory (what/why level), algorithmic strategies (how level), and physical realization (implementation). These frameworks offer valuable insights into how we can effectively dissect and analyze the complexities inherent in this problem. By applying these frameworks, we can pose fundamental questions that lead us deeper into understanding decision-making:

- What is it for? Why does the animal exhibit specific behaviors? Is it for survival, navigation, or evading threats?
- How does this work? How do external stimuli trigger intricate neural responses that give rise to emotions? What neural algorithms and strategies does the brain utilize to make decisions? Where are the specific motor areas or neurons responsible for the animal's behavior?
- After initiating behavior, how does the brain persist in processing and integrating sensory input to formulate subsequent decisions? Does the brain adapt or learn during this

ongoing process? How does this continuous processing influence our subsequent

decision-making?

Despite a general consensus on the significant function of animal emotions, researchers have yet to pinpoint, at a single-cell resolution, the underlying mechanisms at work. In this study, we utilize zebrafish as a model organism to investigate how external stimuli and neural processing give rise to emotions and decision-making at a cellular level, building innovative tools described below. The framework connecting these components includes a zebrafish fish line capable of providing neural activity fluorescence, controlled stimulation through olfactory, UV, or acoustic methods, a lightsheet microscope enabling the recording of hundreds of brain volumes per second at sub-cellular resolution, a behavior tracking microscope, and a verification setup to ascertain the positive/negative valence of affective states and the functionality of behaviors. Last but not least, an analysis pipeline integrates these aforementioned components to bridge the gap between stimuli, affective states, neural activity, and behavior.

Chapter 2: Methods and Results

2.1 Construction of GEVI and GECI fishlines

Larval zebrafish, due to their diminutive size and transparency, offer an opportunity for whole-brain functional imaging. As a vertebrate species, they serve as a prominent model in biomedical research [5]. Zebrafish are easily amenable to genetic editing and exhibit rapid developmental traits. Recent advancements in Genetically Encoded Calcium Indicators (GECIs) and Genetically Encoded Voltage Indicators (GEVIs) have enabled the in vivo imaging of neurodynamics across extensive neural populations.

GECIs are genetically engineered proteins that fluoresce upon binding to calcium ions, enabling the real-time monitoring of changes in intracellular calcium levels. On the other hand, GEVIs, also genetically encoded proteins, alter their fluorescence in response to shifts in membrane voltage, offering a direct means to monitor cellular electrical activity.

Regarding our study, it's pertinent to discuss the specific advantages and disadvantages of GECI and GEVI lines:

2.1.1 GECI:

Genetically Encoded Calcium Indicators (GECIs) are pivotal tools in neuroscience for monitoring cellular activity through calcium dynamics in live cells. One common limitation of GECIs is the relatively slow speed of changes in fluorescence following calcium binding, largely due to limitations in sensor biophysics following calcium binding. Efforts to enhance the Signal-to-Noise Ratio (SNR) often lead to a trade-off with slower kinetics[6]. I acquired three different types of GCaMP8 fish lines from HHMI-Janelia [6]: jGCaMP8 sensors, which consist of jGCaMP8s (with a fast rise, slow decay, and high sensitivity), jGCaMP8f (featuring a fast rise and fast decay), and jGCaMP8m (displaying a fast rise and medium decay). Notably, all

jGCaMP8 sensors exhibit nearly tenfold-faster fluorescence rise times compared to previous GCaMPs [6], enabling the tracking of individual spikes in neurons with spike rates of up to 50 Hz [7]. The detailed specs comparison was reported by Zhang et al[7], listed in Appendix A. In addition to the GCaMP8 lines I imported from Janelia, this study also uses soma:GCaMP7f zebrafish[8] made by other members of the Boyden lab.

2.1.2 GEVI:

Voltage indicators have the potential to record subthreshold potential levels, allowing for direct measurement of neuron membrane voltage across extensive neuron populations with high spatiotemporal resolution. In our investigation, we assessed various voltage indicators, including ASAP3[9], Voltron2[10], Ace-mNeon2, pAce [11], and Positron2[12]. The Positron2 fish line was selected for experimentation due to its superior spike amplitude to shot noise ratio (signal to noise ratio) when compared to Voltron2[10].

Despite its high signal to noise ratio , Voltron2 was excluded from our study because the imaged fish exhibited a lack of neural activities, the underlying causes of which remain to be explored. The kinetics of Voltron2 and Positron2 are estimated to be 1ms, as both indicators utilize the same Ace2 rhodopsin mutations employed in making pAce, albeit with slight modifications involving mNeon swapped for HaloTag expression [11].

The creation of the voltage fish line was primarily inspired by the methodology outlined in the article titled "A general approach to engineer positive-going eFRET voltage indicators" by Eric R. Schreiter et al. The Tg(HuC:Gal4; 3xUAS:Positron2-Kv) transgenic zebrafish line was generated through embryonic micro-injections using the Tol2 transposon system[13] . Zebrafish embryos, at 3 days post-fertilization (d.p.f.), underwent staining processes involving the incubation in fish facility water containing 3 μM JF525-HaloTag for two hours[14]. Subsequently, for Positron2-Kv fluorescence labeling, the fish were immersed in a JF525-HaloTag ligands dye solution for another two hours before imaging.

During the interim period (~4 hours in our experiments) between staining and light-sheet imaging, indicators synthesized could not be labeled with fluorescence dye. This limitation arose because Positron2-Kv indicators necessitate staining with a chemical dye solution to acquire fluorescence [10,12,15]. This duration includes incubation in fresh water to remove dye molecules that failed to bind with the voltage indicators, as well as the mounting of fish in a customized water chamber for imaging.

We have taken measures to stabilize our current fish line, which has been experiencing some health issues and a decline in expected physical activity among certain fish. To enhance the reliability of the fish line, we have segregated the fish derived from different founders. This division applies to both Tg(HuC:Gal4; 3xUAS:Positron2-Kv) and Tg(HuC:Gal4; 2xUAS:Positron2-Kv). The tables (Table 1 and Table 2) below detail the performance and availability of these founder fish. Among the 21 3xUAS:Positron2-kv founders, we calculated their targeted gene transmission by using the number of positive progenies divided by the total number of the progenies. Additionally, we assessed their fluorescent expression in terms of their brightness and uniformity across the brain. We found most of the founder fish did not have consistent or bright Positron2 expressions and that very few had bright and consistent expressions. I also evaluated the health and behavior normality by observing their reactions to external vibrations or food stimuli (paramecia) as shown in Figure 1, and their ability to navigate vertically in a deeper dish as shown in Figure 2. Additionally, I observed the zebrafish's heartbeat and mouth movement, as well as the expression of fluorescent proteins on the side of the brain, while loading the zebrafish larvae into a glass capillary shown in Figure 3.

Table1: GEVI performance evaluation of Tg(HuC:Gal4; 3xUAS:Positron2-Kv) fish founders

Fish Founder ID	Transmission Rate	Inserts	Expression	Availability(Y/N)
1	23/90	single	not as bright	Y
2	28/65	more than 1 or parent homozygous for Gal4	consistent and bright	Y

3	14/32	more than 1 or parent homozygous for Gal4	consistent and bright	Y
4	11/90	lower than 1	inconsistent	Y
5	18/85	single	consistent and bright	N
6	14/21	more than 1 or parent homozygous for Gal4	inconsistent	Y
7	37/90	more than 1 or parent homozygous for Gal4	inconsistent	Y
10	40/88	more than 1 or parent homozygous for Gal4	inconsistent	Y
11	13/80	lower than 1	inconsistent	Y
12	34/90	more than 1 or parent homozygous for Gal4	inconsistent	Y
13	25/90	single	consistent	Y
15	18/85	single	consistent	Y
17	18/85	single	consistent	Y
18	37/85	more than 1 or parent homozygous for Gal4	inconsistent	Y
19	6/75	lower than 1	inconsistent	Y
20	17/85	single	consistent	Y
21	11/70	lower than 1	some consistent some	Y

			barely express	

Table 2: GEVI performance evaluation of Tg(HuC:Gal4; 2xUAS:Positron2-Kv) fish founders

Fish Founder ID	Transmission Rate	Inserts	Expression	Availability
1	No positive fish			
2	No positive fish			
3	No positive fish			
4	No positive fish			
5	No positive fish			
6	No positive fish			
7	No positive fish			
8	Very low brightness			
9	2/45	lower than 1	consistent and bright	Y
10	No positive fish			
11	No positive fish			
12	No positive fish			
13	No positive fish			
14	No positive fish			
15	No positive fish			
16	Very low brightness			
17	No positive fish			
18	No positive fish			

Fish Founder ID	Transmission Rate	Inserts	Expression	Availability
1	No positive fish			
2	No positive fish			
3	No positive fish			
19	No positive fish			
20	23/45	more than 1 or parent homozygous for Gal4	bright and consistent overall, some uneven across the brain	Y
21	No positive fish			
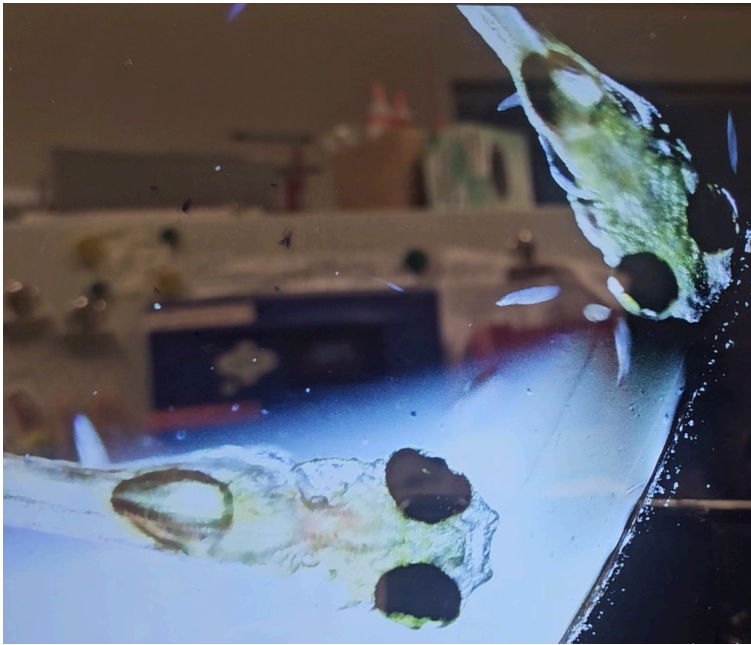
Figure 1. Evaluating the fish response to paramecia
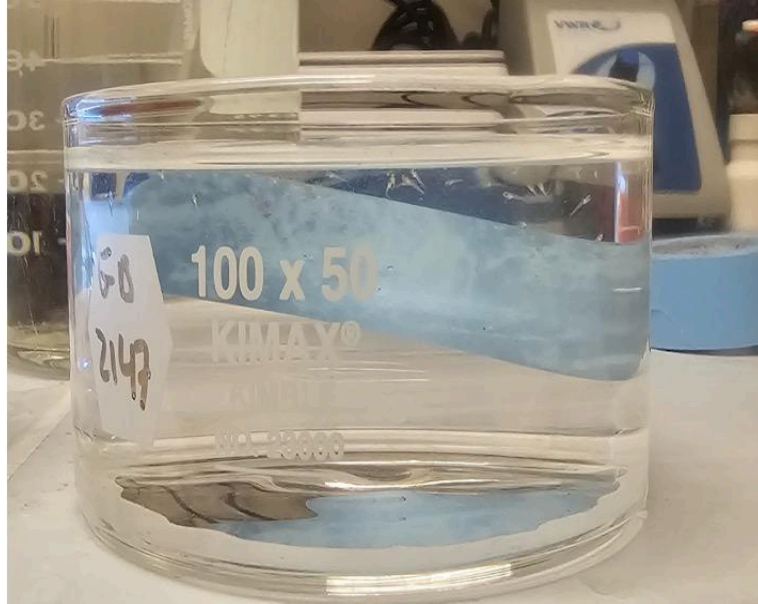
Figure 2. Assessing fish health by observing its behavioral response to external vibration and its vertical navigation in a deeper dish

Figure 3. A 4 days post fertilization (d.p.f.) zebrafish larvae mouth movement and a side view of the brain can be observed by mounting the larvae in a capillary with an inner diameter of 0.8mm.

I found that a majority of the positive Positron2 fish are not swimming as actively as other types of fish, such as those negative for Positron2 or the soma:GCaMP7f fish. This finding is consistent with my colleague Zeguan Wang's report. Additionally, the Positron2 fish with good fluorescent expression appear to be less responsive to external vibration and do not hunt paramecia as expected. They also show behavioral and neural activity variation across the population.

We have identified stripe artifacts in our Positron2 zebrafish under lightsheet microscopy and encountered difficulties in segmenting our voltage imaging data. To address these issues, I am actively exploring various solutions, such as enhancing microscopy design and improving fish lines by using different voltage indicators or double-positive transgenic fish along with my colleagues. These improvements aim to provide deeper insights into the sources of aberrations, reduce systematic aberrations, and enhance neuronal labeling. For example, I have evaluated the double transgenic lines of nuclearRFP/Positron2 and nuclearRFP/somaGCaMP7f. We also aim to use vascular transgenic lines such as Tg(flk:DsRed) and Tg(fli:EGFP) to investigate the impact of blood flow on our image quality further. Additionally, we imaged fixed zebrafish in 4% paraformaldehyde (PFA) and identified the strip artifact as originating from the sample itself.

The fluorescent expression of the fish was assessed by screening different sections while mounted in agarose in a small glass-bottom petri dish or in a rotatable capillary to access the side of the brain under the confocal microscope. The images below showcase some of these confocal observations.

Figure 4 shows pan-neuronal somaGCaMP7f expression in the somaGCaMP7f/nuclearRFP double-positive transgenic line in a 2048x2048 pixel (650 nm/pixel) confocal image. The performance of nuclearRFP is uniform and pan-neuronal across the somaGCaMP7f/nuclearRFP and nuclearRFP/Positron2 double-positive fish lines, as shown in Figure 5. A section of the Positron2 fish brain is also shown in Figure 6, where we evaluated multiple regions of the brain as well as the side of the brain. The Positron2 fish are not as pan-neuronal as our nuclearRFP and somaGCaMP7f fish line. However, we were able to find several fish with relatively wide

expression (about 80% of the brain) across the forebrain, midbrain, and hindbrain regions of the zebrafish.
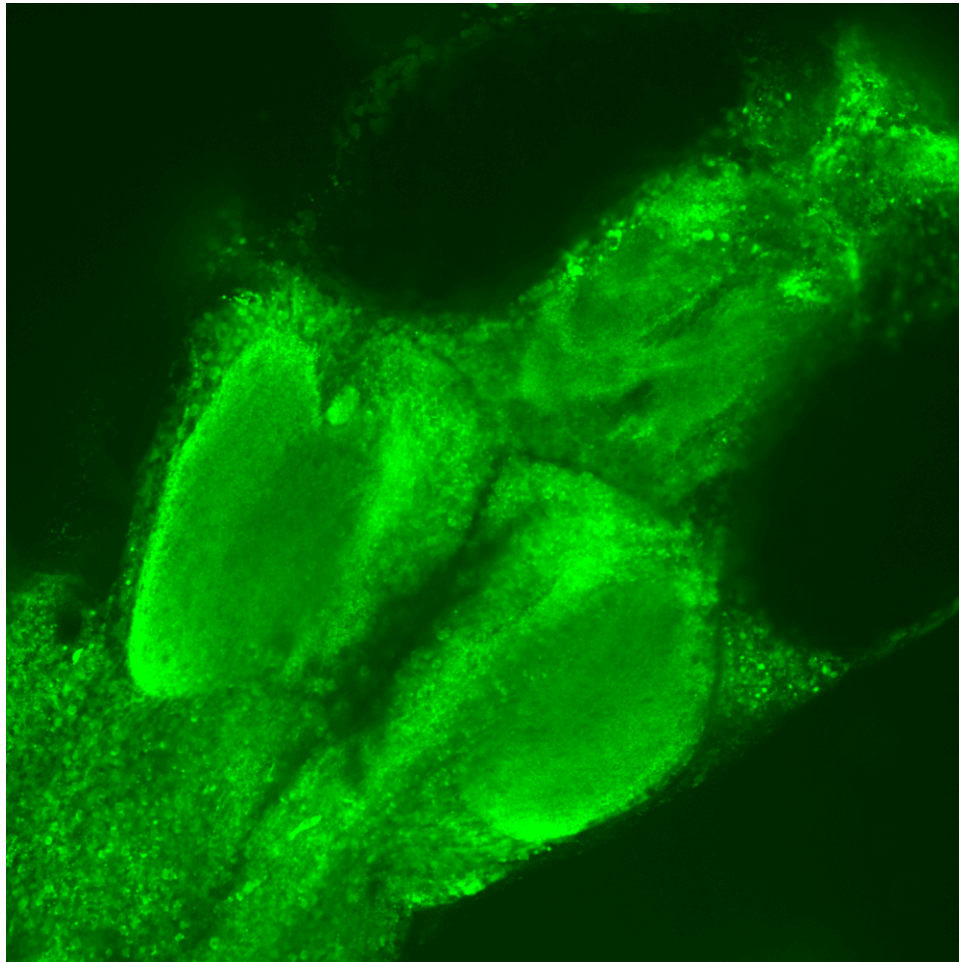
Figure 4. somaGCaMP7f expression in somaGCaMP7f/nuclear RFP double positive transgenic line in 2048x2048 pixels (650 nm/pixel) image
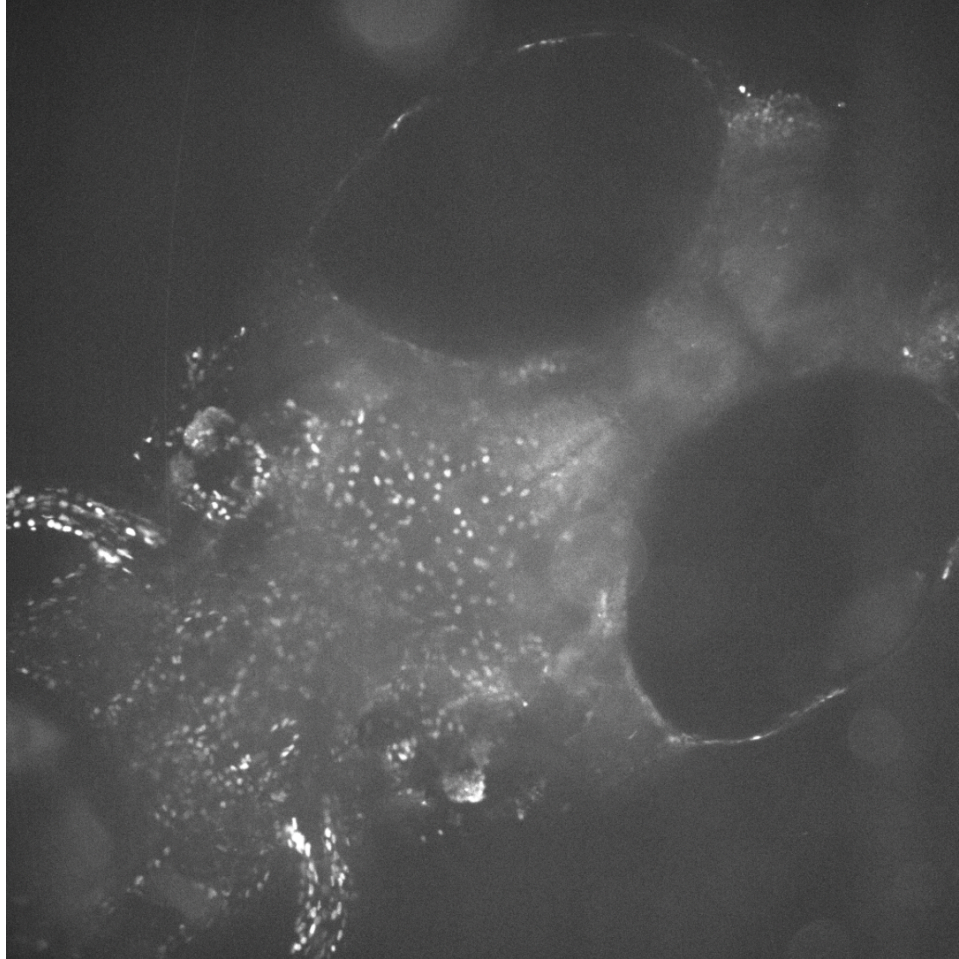
Figure 5. Similar uniformity of nuclear RFP expression is observed in the somaGCaMP7f/nuclear RFP and nuclear RFP/Positron2 double positive fish lines, as demonstrated in 2048x2048 pixel images (650 nm per pixel).
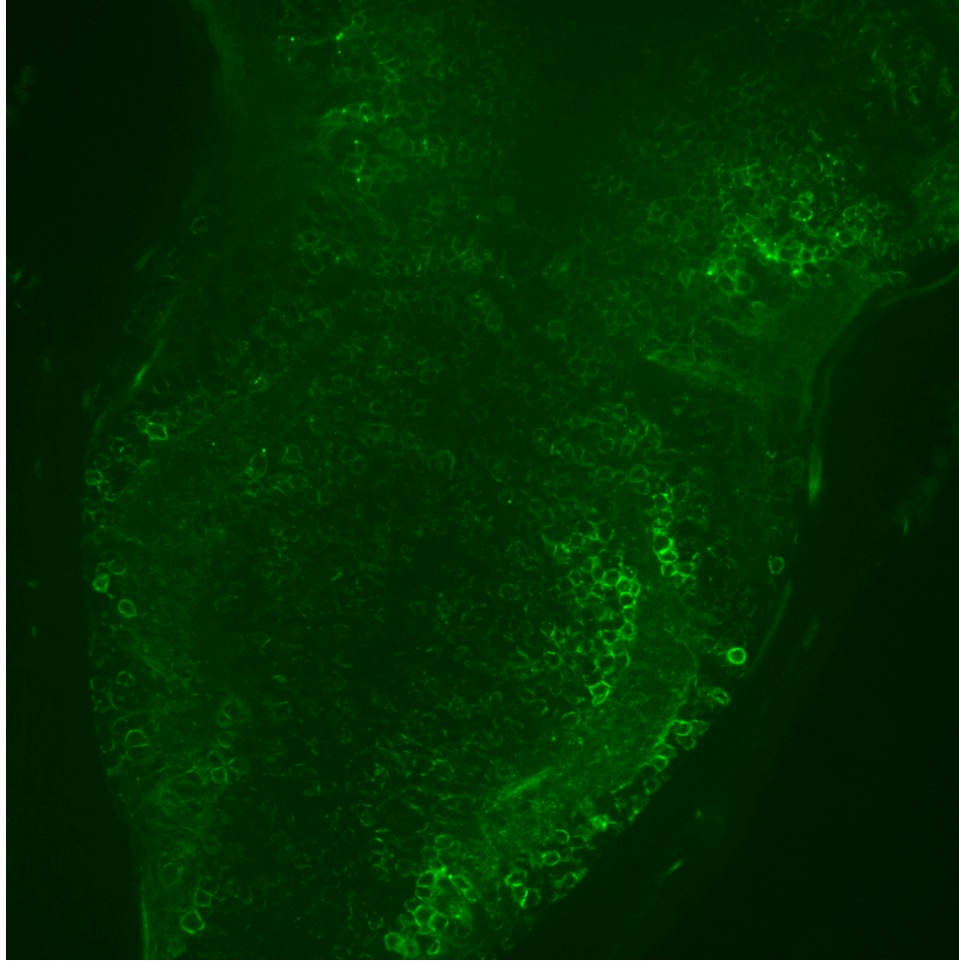
Figure 6. A section of Positron2 fish brain under confocal. Different brain regions (forebrain, midbrain, hindbrain) are evaluated through imaging with a petri dish or capillary. Image is 2048x2048 pixels with 162.50nm/pixel. Fish with wider and brighter fluorescent expression are selected for lightsheet imaging in our study.

To optimize the performance of GEVI in zebrafish, it is imperative to devise a rapid and reliable fish mounting method to minimize the duration between dye staining and imaging, which we will discuss in the next section. In summary, both GECI (Genetically Encoded Calcium Indicators) and GEVI have distinct advantages and disadvantages. Calcium indicators offer ease of use, requiring less stringent screening processes due to established lines and not necessitating

additional dye protocols for fluorescence acquisition. Their biological impact and kinetics are well-studied, they enable pan-neuronal expression with activity, and numerous datasets from researchers utilizing such indicators are accessible and registered to ZBrain[16,17], facilitating comparative analysis and biological inferences.

On the other hand, GEVI holds promise in measuring subthreshold potentials and direct membrane voltage, alongside facilitating the observation of rapid neurodynamics due to its fast kinetics. We are working on enhancing GEVI expression throughout the zebrafish's entire brain volume to enable comprehensive neuronal activity recording. Additionally, we are actively seeking alternative molecules with slower kinetics that could enable ground-truth neural activity measurement at 200 Hz, the volumetric rate of our current Dual Objective Light Sheet (DOLS) setup. It is evident that the injected plasmid and the fluorescent dye used for the Positron2 fish may be toxic, leading to physical inactivity and a lack of navigation and hunting behavior compared to healthy fish of the same age. We are in the process of stabilizing Tg(HuC:Gal4; 2xUAS:Positron2-Kv) and Tg(HuC:Gal4; 3xUAS:Positron2-Kv) by outcrossing founders with relatively better fluorescent expression. Additionally, we are exploring alternative voltage indicators such as the new Solaris[18].

Although my work evaluating the performance of progenies of F1 Positron2 fish injected by my colleague Zeguan Wang has not yielded a bright, pan-neuronal, healthy voltage indicator line, it has been instrumental in helping us adapt more efficient screening methods. For example, screening each founder separately gives us more control compared to the previous method of having all 21 fish mate at once. Understanding the likelihood (transmission rate) of the founder fish giving Positron2-positive progenies helps us determine which founders to use for breeding the next generation.

Observing the rare expression among the population, individual variability, and behavior issues of the Positron2 fish has helped us pinpoint future directions for improvement. This includes stabilizing the existing line, trying out new indicators, or exploring other driving methods.

After communicating with Adam Amsterdam at the Koch facility, he suggested we try a doxycycline-inducible system. This system allows researchers to control gene expression with the administration of doxycycline, enabling the activation or suppression of specific genes at desired times and locations. This method is beneficial for studying genes that may be toxic or harmful if expressed continuously, as it permits precise control over gene expression timing and intensity, minimizing potential developmental or physiological disruptions.

2.2 Sensory stimulation and behavior recording

Zebrafish larvae have a diverse range of sensory capabilities, allowing them to detect and react to multiple types of environmental stimuli, e.g., olfactory [19–22], audio [23–27], visual stimulus [28–30]. We have developed a zebrafish stimulation setup for all three types of stimuli.

2.2.1 Olfactory stimulation

Our olfactory stimulation uses a customized self made stimulation chamber. This chamber is inspired by this existing optofluidic chamber design, customized for our imaging needs and fabricated at MIT Nano[31]. Table 3 below shows a ten step process I underwent to fabricate a zebrafish stimulation chamber at MIT Nano. Briefly the process include design and procure photo mask, preparation of silicon wafer, spin coating SU8, conducting photolithography using a photomask and exposer/mask-aligner, multiple rounds of washing in developer solution to remove uncured SU8, bake the developed wafer again to harden the patterned SU-8, prepare a PDMS mixture and pour it onto the patterned SU-8 wafer, cure the PDMS in an oven, After curing, carefully peel off the PDMS replica with the microfluidic channels from the SU-8 master, punching channels for microfluidic stimulation and fish loading. The major equipment used in this process are shown in Figure 8. Additionally, I set up microfluidic controller as well as channel punchers tailored to the size of our zebrafish larvae as shown in Figure 7 .

MIT.nano: Process Submission

Title:	SU8 PDMS Stimulation Chamber Process
User(s):	Caroline Zhang carol410@mit.edu

Starting
Material: Standard 4" silicon wafers, purchased from the Attention to Details Wafer Company

(include any history of past processing in other labs. If too long, add that as a step 0 below)

Step	Coral Tool Name	Details	Notes
0	Fineline Imaging Photomasks	Designing and procuring photomasks based on microfludic chamber design	
1	SU8-Spinner-Hood	Solvent clean wafers as needed	
2	Spinner-SU8	Coat with SU8 (thickness = 400um)	
3	SU8-Spinner-Hood	Prebake on hotplates, temperature and time depend on SU8 thickness / see datasheets	
4a	EVG	Expose with mask aligner	
4b	DirectWrite-MLA150-*	Alternative direct write	
5	SU8-Spinner-Hood	Post exposure bake, according to datasheet	
6a	Spinner-SU8	Option 1: Develop on coater with plumbed developer	
6b	SU8-Spinner-Hood	Option 2: Develop in dish	
7	SU8-Spinner-Hood	Hard-bake SU8	
8	Mixer-PDMS-Degas	Mix up pdms and pour	
9	Oven-PDMS	Cure	
11	Creating Microfludic chanels	Punching microfludic and Fish loading channels	
10	Asher-SoftLitho	Surface modify PDMS if bonding to a glass slide	

Table 3. MIT Nano cleanroom microfluidic chip protocol
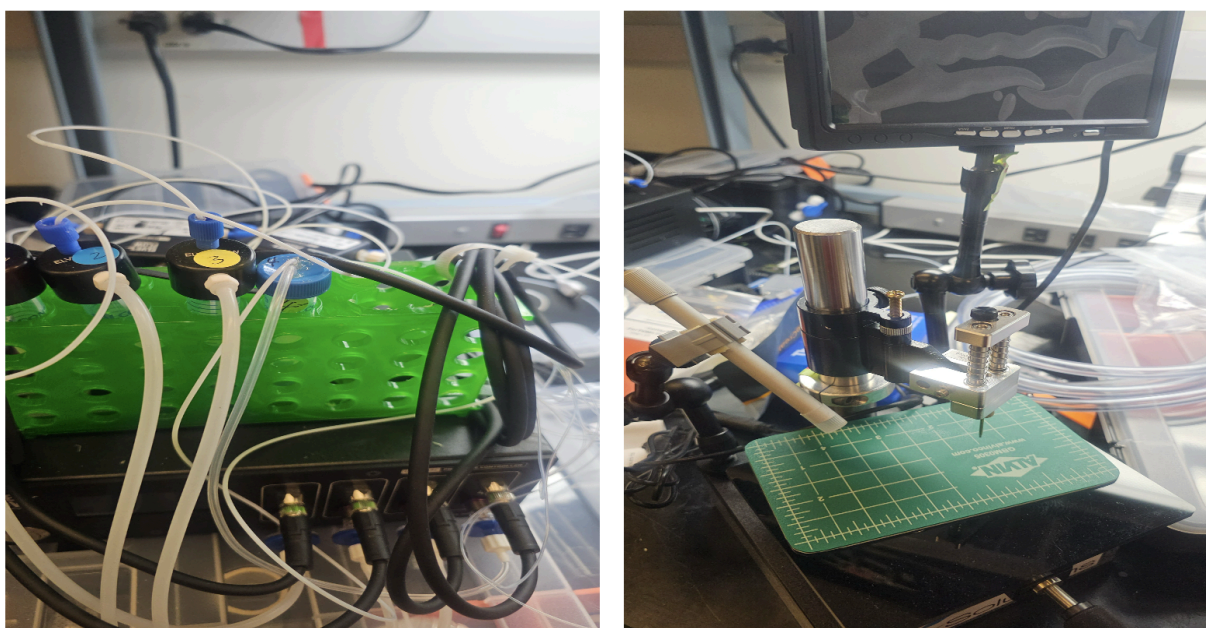
Figure 7. (Left) Microfluidic stimulation pump and controller and (Right) Microfluidic channel puncher tailored to our zebrafish larvae
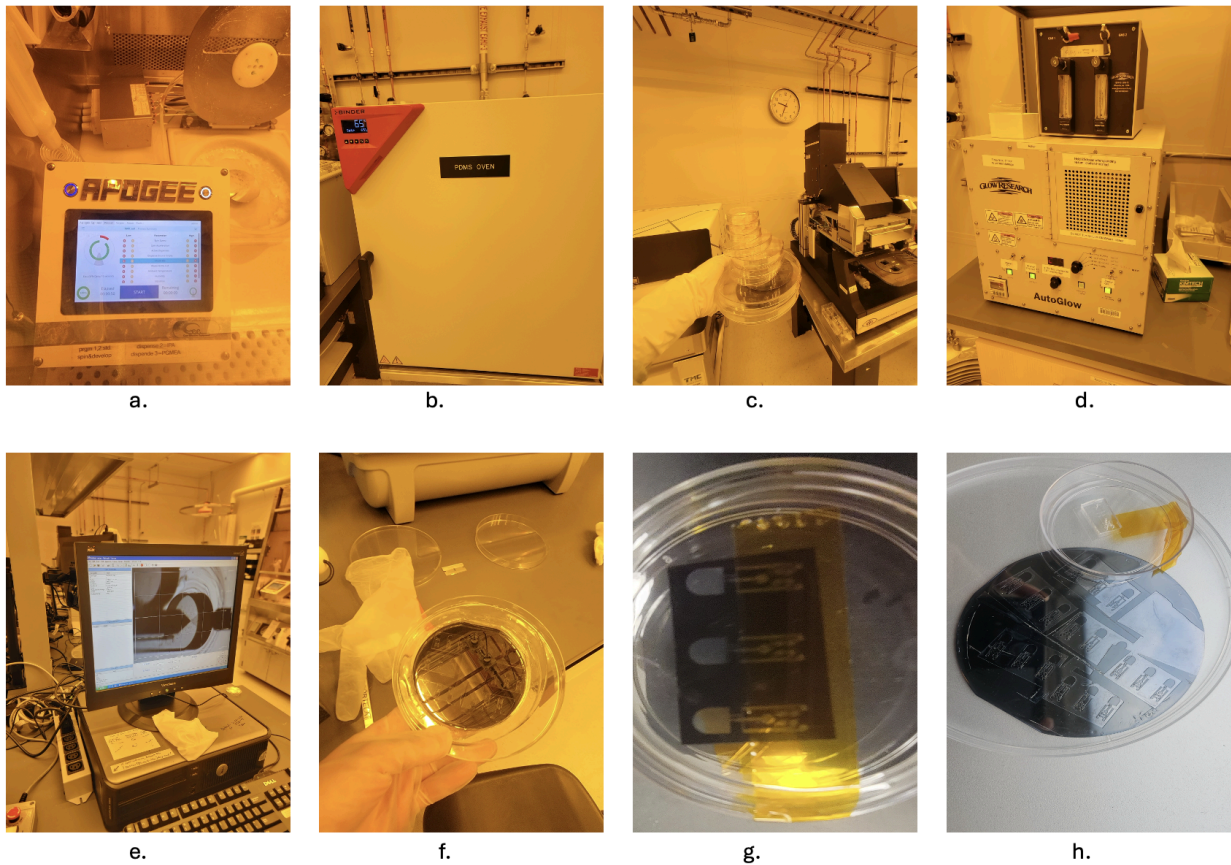
Figure 8. Protocols used to make zebrafish microfluidic simulation chip: a. SU-8 spinner hood b. PDMS oven c. UV exposer d.PDMS plasma cleaning usher e. channel depth meter f. SU-8 mold on a silicon wafer g. transparency film to make SU-8 mold h. SU-8 mold on a silicon wafer with a PDMS microfluidic chip on the top corner of the picture

This new olfactory design offers several advantages over previous designs, primarily due to its compact size, deliberate measures to minimize motion artifacts, and precise control of odor delivery [32] [33]. Figure 9.a illustrates the PDMS microfluidic module published by Sy et al[31], featuring elements for securing the larvae head, a tail chamber enabling tail behavior, as well as fluidic and fish loading channels. An additional side channel was incorporated to equalize the

pressure differences of the stimulant, thereby reducing motion artifacts[31]. I revised the design by changing channel depth and chip dimensions to suit our needs and fabricated the chip shown in Figure 9.b. at MIT Nano.

Moreover, the simplified syringe-based fish loading method through the outlet fluid channel eliminates the need for additional embedding, significantly reducing the time required for sample preparation. This expedited fish preparation process can address the challenges related to the sparse expression problem associated with zebrafish positron2/voltron2 protocols, where a fluorescent dye[14] needs to be applied just before imaging. Furthermore, the consistent positioning of the fish, avoiding manual embedding, can ensure uniform imaging coordinates across the entire fish population, streamlining the image processing workflow.

Next, we plan to use BIO-133, a polymer with refractive index close to n=1.33 of water to substitute the PDMS to minimize the aberration. Han et al characterized the suitability of BIO-133 for optical imaging in microfluidic/immobilization setups, particularly in time-lapse volumetric imaging of cellular dynamics using lightsheet and superresolution microscopy [34]. Under MIT Nano's guidance, such polymer has been added to clean room chemical inventory and a protocol to make BIO-133 olfactory stimulation chip has been approved. The process resembles the protocol shown in table 3, with the exception that the microfluidic chip would be cured in the EV aligner, not baked. Blank transparency films are employed to shield the polymer from undesired oxidation and impurities.

I have also modified the stimulation and olfactory setup to be compatible with the dual objective lightsheet microscope. This setup includes sample holders for both sound and olfactory stimuli. As illustrated in Figure 10, light enters from the sides and the images are captured by the objective on top. The glass coverslip at the bottom facilitates tail recording and behavior tracking, while the microfluidic chip depicted can deliver chemical olfactory stimuli.
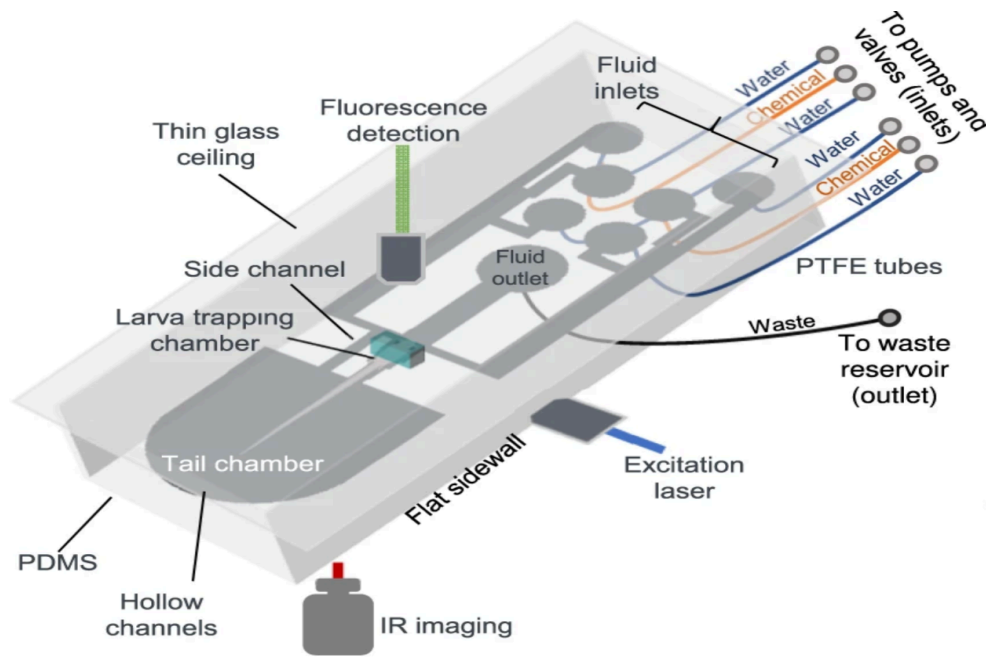
a
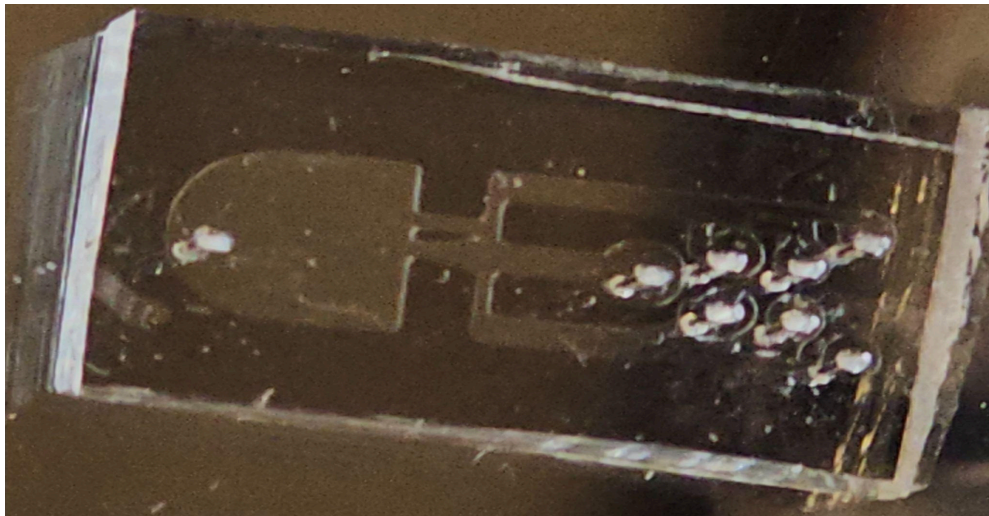
b

Figure 9. a) microfluidic chip compatible with whole-brain and tail imaging with fluidic and fish loading channels published work by Sy et al [31] b) A self-made microfluidic chip at MIT Nano customized to the age of our fish.

We used cadaverine as an aversive odor and l-alanine amino acid as an attractive food odor, with fish water serving as a neutral stimulant to test the microfluidic delivery system, as shown in

Figure 7 (left). Our aim was to precisely control odors, hypothesizing that cadaverine triggers a negative affective state and prompts escape behavior, while l-alanine induces a positive affective state, leading to foraging behavior (swimming towards the odor). We anticipated that fish water alone, serving as a neutral stimulus, would not elicit escape or foraging behavior in the fish. Conversely, our hypothesis suggested that pre-administering a positive or negative odor would evoke a corresponding positive or negative valence affective state in the animals. As a result, we expected to observe chasing and escape behaviors even when solely exposed to a neutral stimulant.

However, challenges such as leaking channels during the loading of the fish were encountered, indicating the need for further refinement of the experimental setup before drawing any biological conclusions. To address this issue, I plan to use our specialized channel puncher needle (shown in Figure 7, right) at MIT Nano to seal the channels, as they are better equipped for soft lithography work.

Future experiments will focus on improving the microfluidic delivery system and conducting more trials to validate our hypotheses. By overcoming the technical difficulties and refining our methods, we aim to achieve reliable and reproducible results that will enhance our understanding of odor-induced affective states and behaviors in fish.

2.2.2 UV and sound stimulation

We built a customized stimulation chamber using 3D-printed frames and coverslip-glued sides and bottoms, enabling simultaneous imaging and behavior tracking. The left panel of Figure 10 displays the embedded fish within the UV and sound stimulation chamber, allowing us to record tail behavior using an IR camera. The right panel of Figure 10 , I attached the speaker to the side of the zebrafish water chamber, facilitating the delivery of sound stimuli. Figure 11 shows how I delivered different waveforms and frequencies of sound stimulation using a function generator.

I plan to slightly adjust the dimensions of the zebrafish holder to maximize the amount of the tail released during imaging for the next batch of fish holders, enabling more precise behavior

recording.This modification would facilitate distinguishing between J and C turns, as shown in Figure 12, potentially involving the releasing of side fins to allow multi-point pose tracking[35].
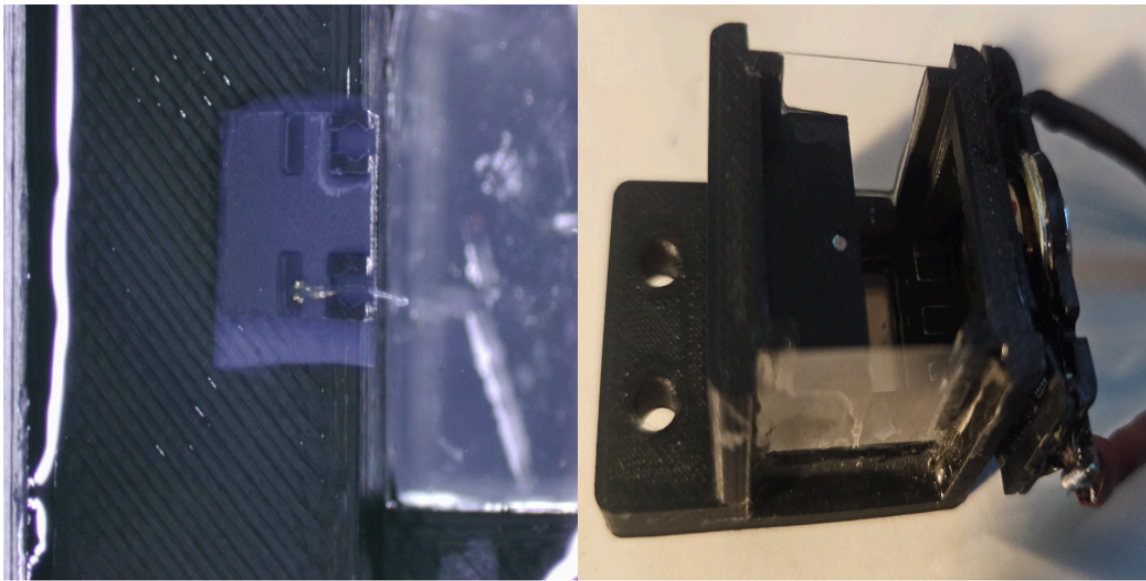
Figure 10. schematics of the zebrafish UV sound stimulation chamber with transparent side and bottom windows allowing lightsheet and behavior camera recording. On the right panel the speaker is glued to the side to provide sound stimulus and in the middle a UV LED is placed to provide UV stimulation
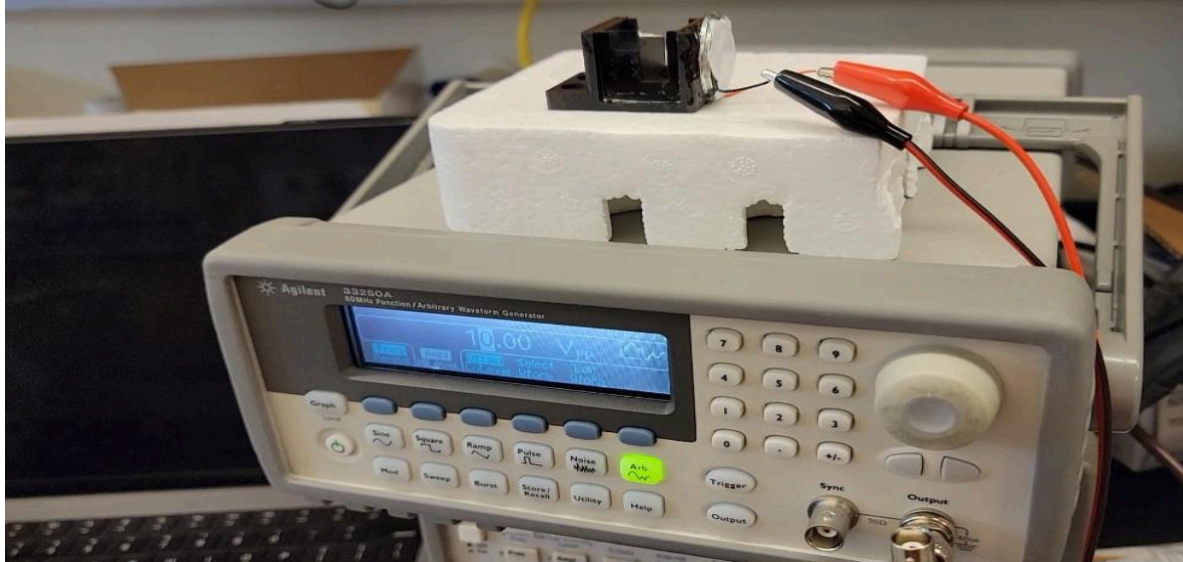
Figure 11. A function generator is used to stimulate zebrafish larvae with sounds of various waveforms and frequencies
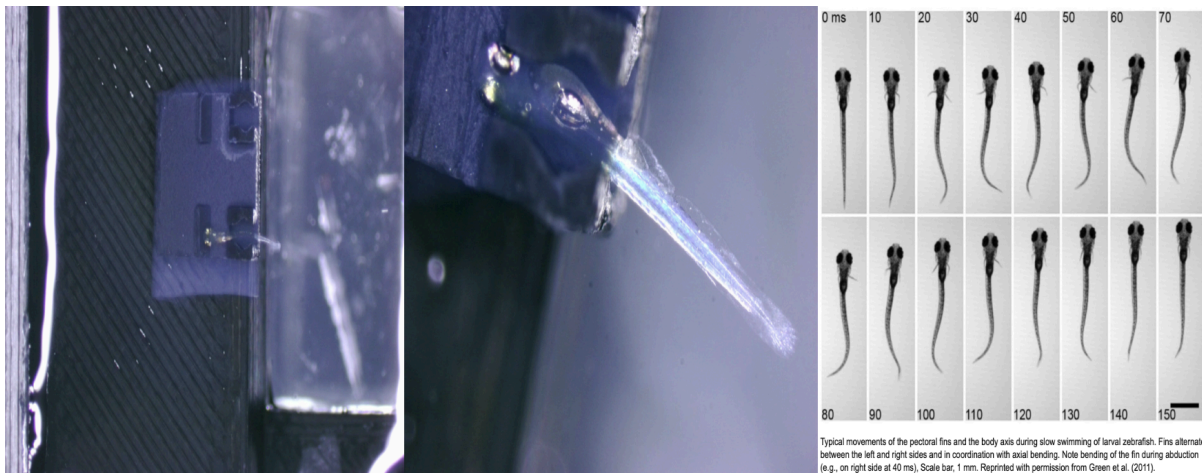
Figure 12. Fish embedding position and fish holder dimension can help distinguish J turns from C turns. These turn types are demonstrated by Green et al [36]. Adjusting the design of the fish holder and embedding geometry can allow multi-point pose tracking for a detailed analysis of fish behavior

I also further modified the stimulation and olfactory setup to be compatible with the dual objective lightsheet microscope. This setup includes sample holders for both sound and olfactory stimuli. As illustrated in Figure 13, light enters from the sides and the images are captured by the objective on top. The glass coverslip at the bottom facilitates tail recording and behavior tracking, while the microfluidic chip depicted can deliver chemical olfactory stimuli.

Figure 13. Revised olfactory stimulation setup tailored to our dual objective lightsheet design, combining a sound stimulus chamber and an olfactory chip. The setup features a coverslip window at the bottom for tracking tail behavior, side windows for light sheet illumination, and a modified microfluidic chip for delivering stimulants.

2.3 Neural activity recording

Researchers have turned to functional imaging to study both neural activity and behavior at the same time. Light-sheet microscopy (LSM) is a promising technique for volumetric fluorescent imaging, as it specifically excites and efficiently images fluorophores in a two-dimensional (2D) focal plane, thus offering high throughput, good optical sectioning capability, and low phototoxicity, while maintaining good spatial resolution (i.e., down to 0.3 μm, lateral meaning x-y)[37–40]. Using conventional LSM, whole-brain, cellular-resolution calcium imaging has been achieved in larval zebrafish, at a volumetric imaging rate of 0.8-3 Hz [41,42]. However, it is difficult to improve the speed of conventional LSM to a volume rate that can be used for voltage imaging, while maintaining the 3D-FOV required to image a whole larval zebrafish brain (~800×370×200 μm³) at cellular resolution [37,39,40]. This difficulty arises from two causes: (1) it is challenging to enhance the scanning speed of the image plane, and (2) cameras exhibit limited frame rates at the necessary camera field of view (defined as the number of row and column pixels captured in one frame). To enhance the scanning speed of LSM, many strategies have been proposed[43–54]. One of them is remote refocusing [43,44], which rapidly shifts the system's focal plane at a remote site using a tunable lens[46], translational tertiary objective lens[45], or translational mirror[47,48]. However, the additional aberration from tunable lenses limits the system's numerical aperture (NA) and two-dimensional field-of-view (2D-FOV, defined as the area that a microscope can image in a single two-dimensional focal plane). Spherical aberration from refocusing can be eliminated using a translational tertiary objective lens[45] or a translational mirror[43,44] at a remote site. However, scanning the tertiary objective lens has the same scanning range and speed limitations as encountered in conventional LSM. Previous studies used commercial mirrors that are several grams in weight and actuators that are designed for heavier loads (such as objective lenses), and thus achieved <100-Hz scanning rates and <100-μm scanning range[47,48].

2.3.1 Single Objective Light Sheet Microscope (SOLS)

Among these remote focusing methods, oblique plane microscopy (OPM)[49–54] or SCAPE[55,56] can also relieve the scan rate bottleneck of LSM. OPM or SCAPE uses a single objective lens

(referred to as primary objective) both for illumination and detection without additional objectives surrounding the sample, which makes the set up versatile to different sample geometries such as our zebrafish olfactory stimulation chip, intact rodent brain and multi-well plates. SCAPE and OPM laterally sweep an oblique-aligned focal plane using remote galvo or polygon mirror scanners, allowing volume scan rates up to the maximum scan rates of these mirror scanners. SCAPE 2.0[55] can scan a 197x293x78μm^3 volume at a high rate of 321 volumes per second (VPS), or a 345x278x155um^3 volume at 100 VPS, but the oblique alignment between the secondary and the tertiary objectives has limited the effective NA to 0.35, which means far (~10x) less light collection than, say, a 1.0 NA lens – challenging, given that voltage imaging is far lower in signal-to-noise than calcium imaging. To increase effective NA, several new OPM configurations were recently proposed, where water chambers[49] and customized objectives [50,51] were used to reduce the misalignment angle between the light cones of the secondary and the tertiary objectives. We revised the SCAPE design by incorporating a specifically designed, glass-tipped tertiary objective lens [57] enabled an $800 \times 420\mu m^2$ 2D-FOV at NA=0.97 in OPM. This resulted a 3.5 times 2D-FOV reported by SCAPE 2.0. However, this glass-tipped objective lens still causes aberrations at the edges of large 2D-FOV's (e.g., >500 μm), as only the center $\Phi 450$ μm^2 of its 2D-FOV is optimized for diffraction limited resolution. This is evident through our fluorescent bead (0.2um size) images using this microscope, which shows more clarity in the center FOV and are blurred at the edges in Figure 14. In the current alignment, our pixel size is about 81nm. The Full Width at Half Maximum (FWHM) is about 244nm at the center field of view, which is our current resolution in xy plane. The point spread function (psf) in XY dimension is also plotted in Figure 14. We still need to fine tune our alignment to reduce aberration of our single objective lightsheet system described in the sections below.
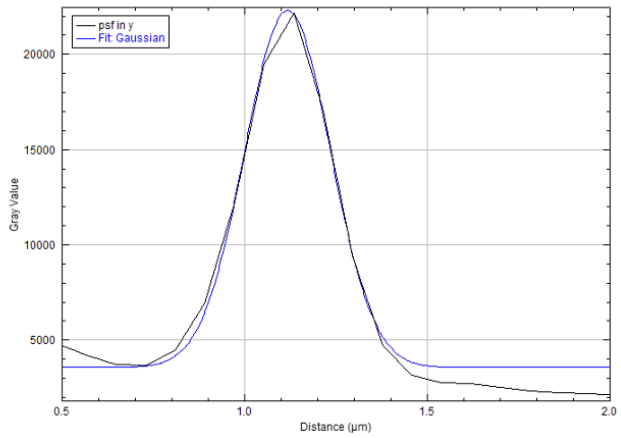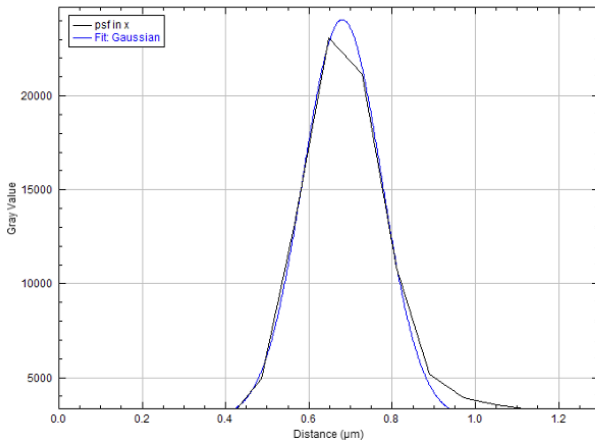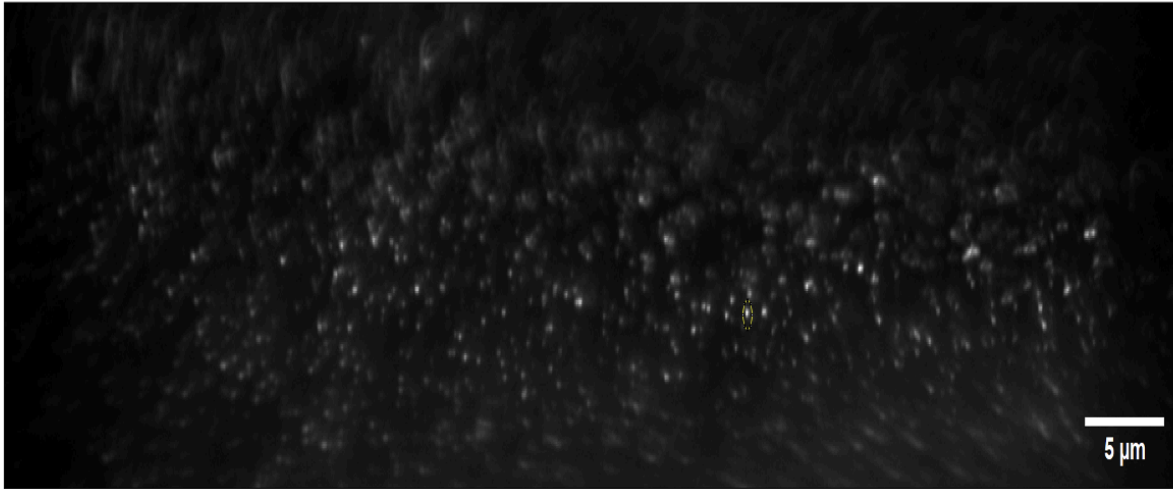
Figure 14. 200 nm fluorescent bead imaged under our single objective lightsheet with AMS-AGY v2 "King Snout" objective [58]. It is evident the center of FOV is better resolved compared to the edges of FOV. We are working to fine tune the alignment to enhance resolution across the filed of view. The bottom panels depicted the psf in x and y.

In addition to revising the SCAPE design to improve the field of view (FOV) and the effective numerical aperture (NA), we identified multiple aspects of the SCAPE 2.0 setup where optical

engineering could be improved to optimize alignment and usability. The following enhancements were made:

1. We coupled all illumination beams into a single-mode fiber, enabling plug-and-play extendibility with multiple-color fluorescence microscopy without the necessity of additional alignment. This improved upon the original SCAPE 2.0 design. A beam expander telescope and an additional objective were used in combination with a Thorlabs 3-axis fiber launch system to precisely focus the beam to the tip of the fiber, as shown in Figure 15.
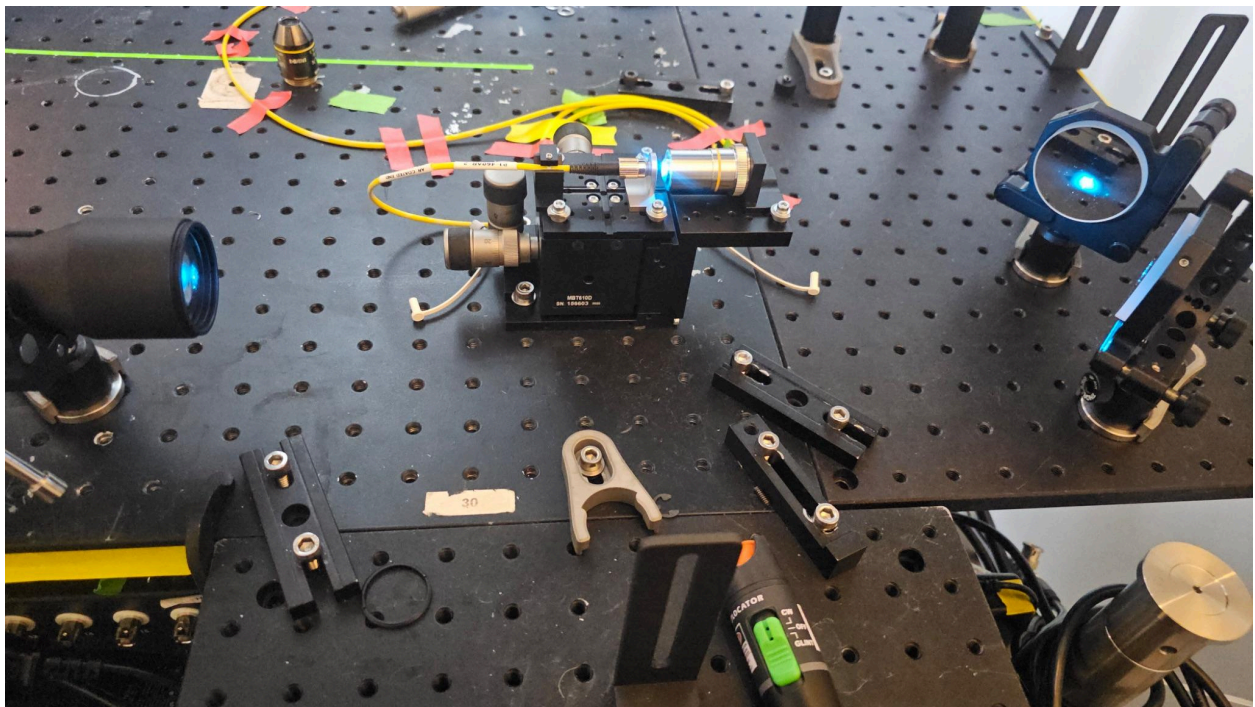
Figure 15. Updated fiber launching setup to enable plug-and-play extendibility with multiple-color fluorescence microscopy

2. We integrated a new flat-top beam shaper consisting of multiple refractive beam shaping optical components, as shown in Figures 16 and 17. This increased light shaping efficiency while relaxing the requirements for input beam wavelengths compared to the Powell lens approach. The Powell lens used in the SCAPE 2.0 design had an intrinsic problem of a fringed beam on the edge. Figure 17 shows the flatter beam profile created by the new pi beam shaper component.
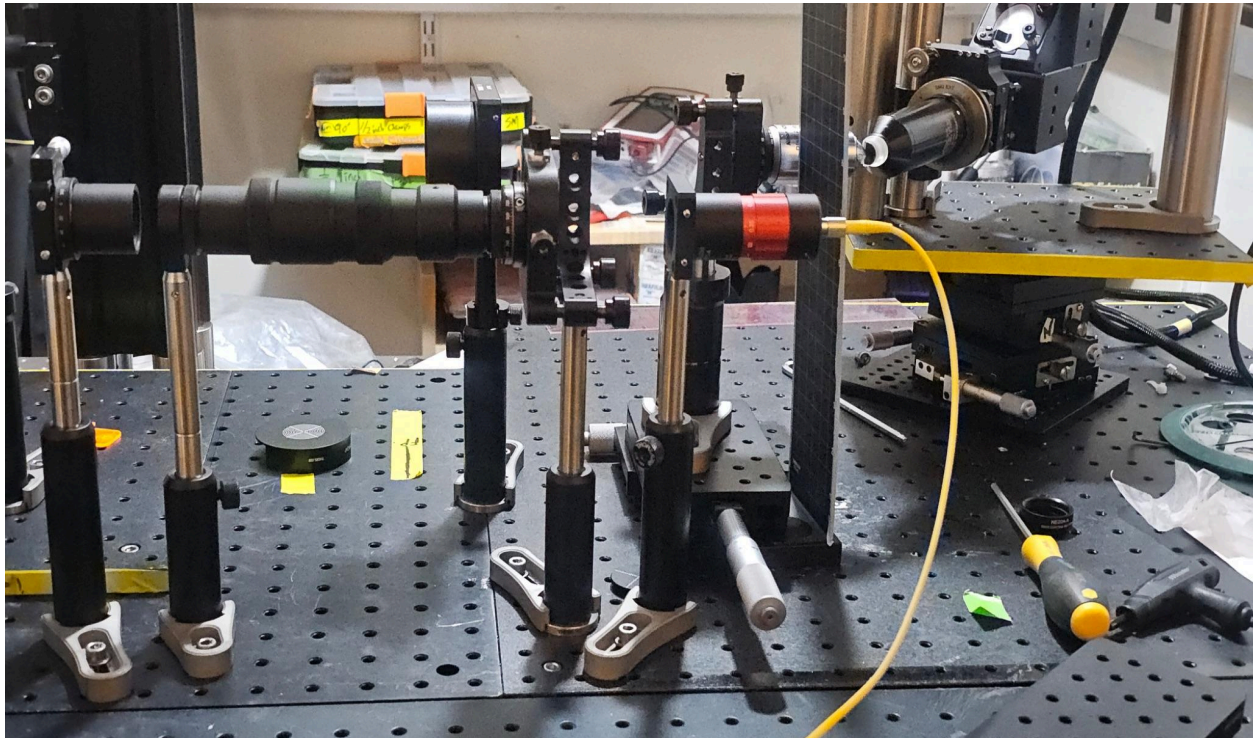
Figure 16. flat top beam shaper[59] that creates uniform flat beam profile included in our current design

File   Device   Palettes   Average   Filter   Camera   View   Setup   Support

Clip[a]	13.5%
Clip[b]	50.0%
Running #1 LCM.10	
Major	7272.4 um
Minor	7194.2 um
Mean	7259.2 um
Eff_2W	6981.6 um
Ellip.	0.99
Orient.	0.00 deg.
Crosshair	0.0 deg.
Xc	675.0 um
Yc	-687.7 um
Centroid: [absolute] Rc	963.6 um
ADC Peak %	71.2%
Plateau Uniformity	0.18
Image zoom	1

Image valid   Frames Good:1278 Bad:70   USB2
HyperCal engaged.   Baseline: 4.77 %   Baseline STD: 0.44 %
4.0 FPS   Frames averaged: 0   ADC Offset: -440 DNs

Zoom: 1

Relative Power: 0.00   Full Range = 2
(Trigger off) delay = 0.000 ms
Imager Gain = 1.0
Exposure time = 100.0 ms (Auto)   (? use less attenuation ?)

2Wua @ 13.5 %	7194.2 um	2Wva @ 13.5 %	7272.4 um
2Wub @ 50.0 %	6457.7 um	2Wvb @ 50.0 %	6317.4 um

Peak = 53.6 %, B = 4.8 %,Scale = 1200.0 um/div

Peak = 58.5 %, B = 4.8 %,Scale = 1200.0 um/div

Figure 17. Flat top beam created by pi beam shaper measured with DataRay beam profiler
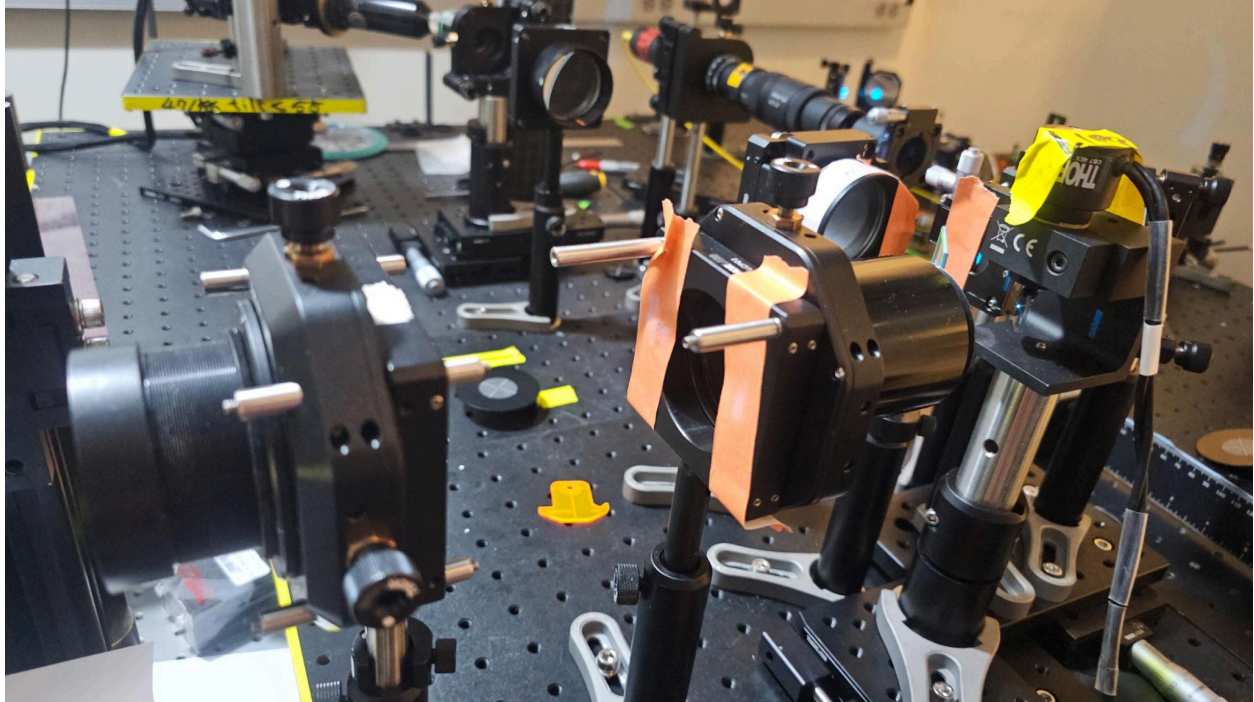
Figure 18. A scan lens with a larger FOV is used in our current design without a cage system. The objective tube lenses have also been updated to match our current design.

3. We used a scan lens with a larger FOV to replace the original design, matched with our glass-tip tertiary objective lens design with reduced field curvature at the edges, as shown in Figure 18. We also updated the objective tube lenses to match manufacturer specifications and the specs of the new scan lens. The illumination telescope components and the detection telescope components were detached from the original cage design to enable more precise alignment.

4. I customized a 6-axis sample stage allowing more diverse sample configurations and adjustments, shown in Figure 19. SCAPE has an oblique plane, which tilts the coordinates of the images. This 6-axis sample stage helped revert the image to normal coordinates. Although this can also be achieved in software, a multi-modal stage capable of tilt correction would make

downstream analysis easier and provide more tolerance for fish mounting position. As shown in Figure 3, a tilted fish brain complicates downstream image registration.
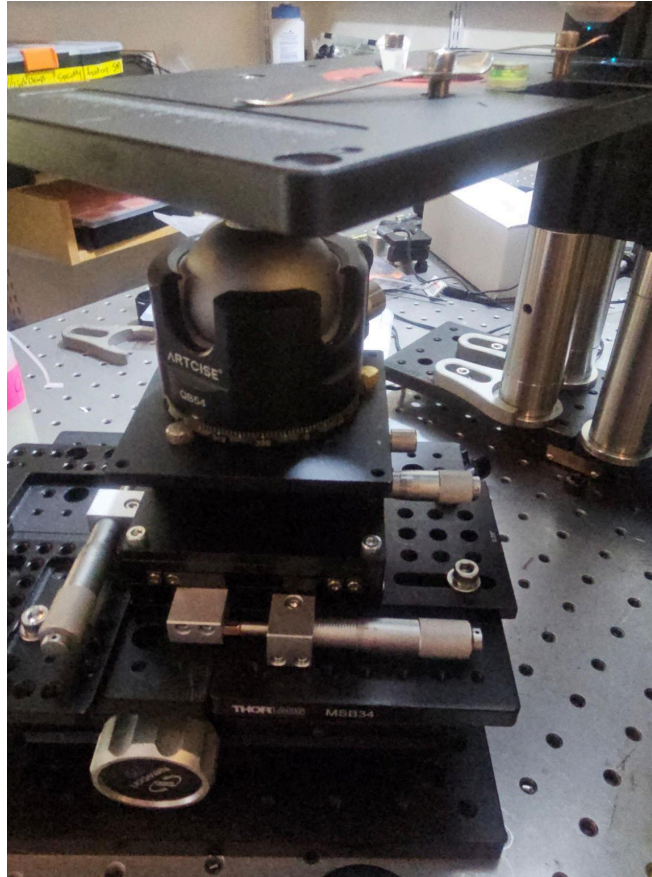
Figure 19. Customization of a 6-axis sample stage allowing more diverse sample configurations and adjustments

5. We updated the sliding lens unit, galvo, and dichroic mirror mounting method to allow more precise alignment, as shown in Figure 20. The location of the sliding lens in the SCAPE 2.0 schematic is critical for determining lightsheet angle and beam offset at the primary objective back focal plane. The galvo needed to be precisely aligned with the incoming beam, the illumination, and detection telescope to achieve better image quality. The dichroic mirror position also needed to be precisely controlled, especially with multiple illumination beam

wavelengths. We updated the dichroic mirror mount using Thorlabs FBTA mount, allowing fine rotation and tip/tilt adjustment, as shown in Figure 21.
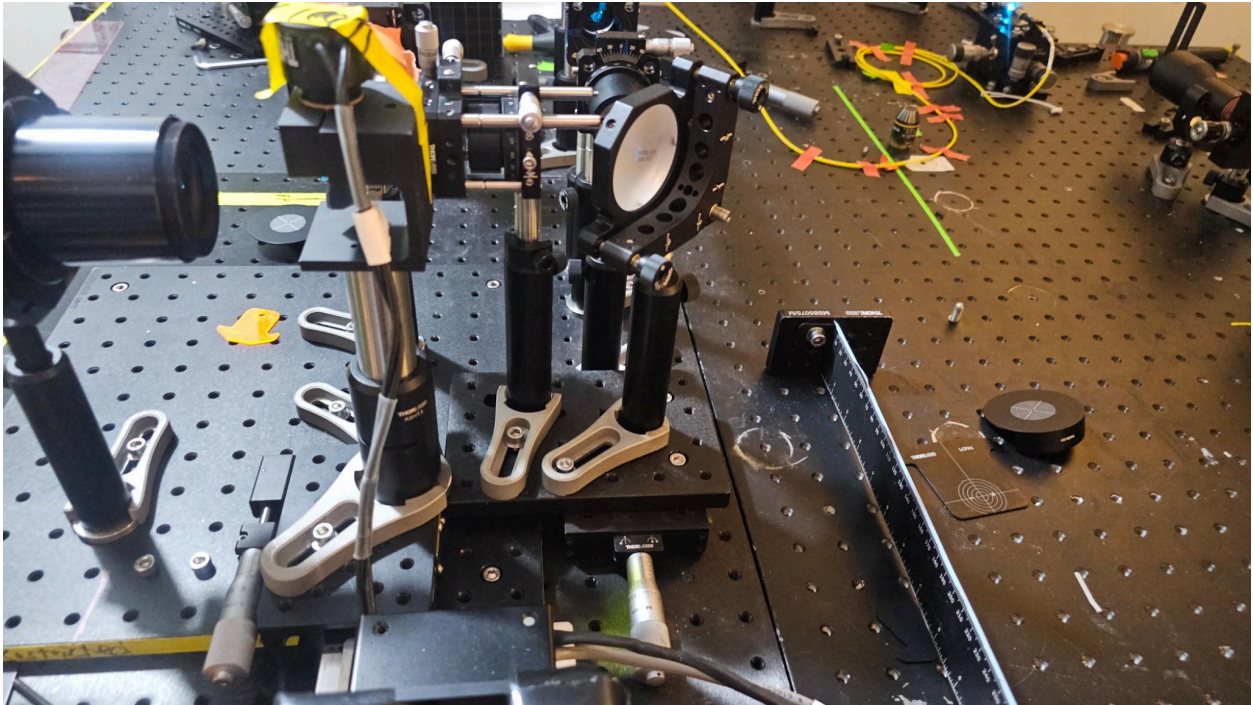
Figure 20. The updated precise microcontrollers for the sliding lens unit and galvo mirror
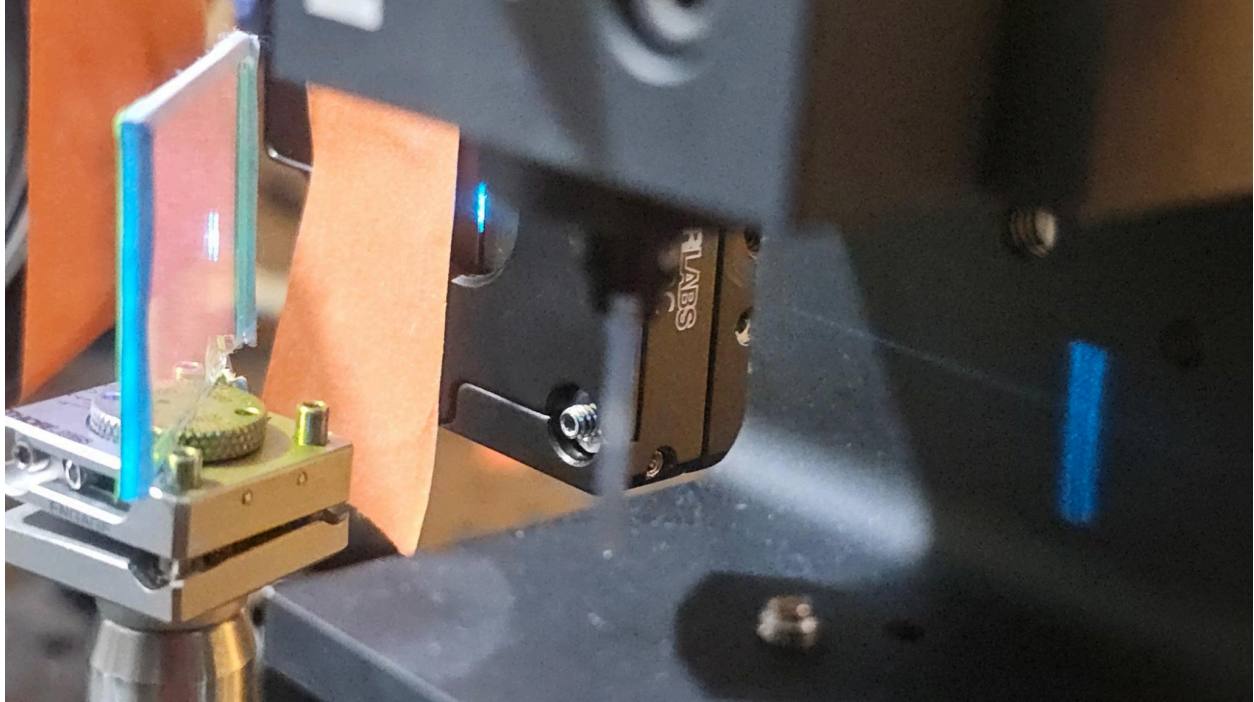
Figure 21. Updated dichroic mirror mount to allow fine rotation and tip/tilt alignment

6. We updated the primary objective mounting platform to provide more stability compared to the original SCAPE setup, as the former design seemed unstable with a heavy high NA objective lens, as shown in Figure 22.
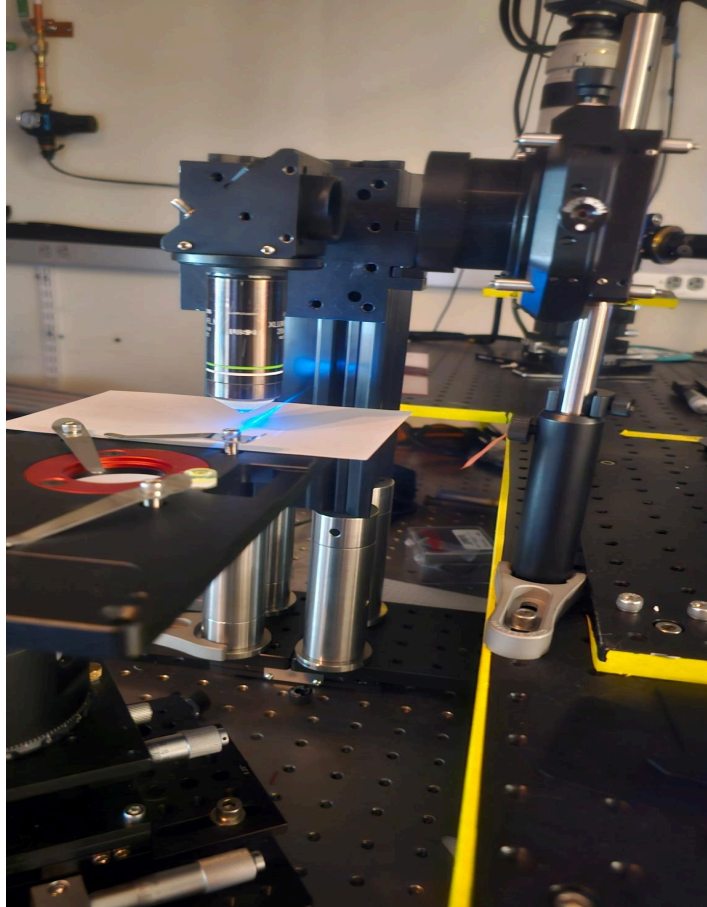
Figure 22. Updated primary objective mounting to stabilize the system

7. We updated the remote focusing and tertiary objective mounting method to enable more precise alignment. The tertiary objective was placed on an x-y-z-radial 4-axis stage to allow fine alignment, as shown in Figure 23. The remote focusing objective was placed on top of a two-axis micrometer controller and mounted in a kinematic optic mount to allow precise alignment. The angle and positions of the remote focusing objectives were critical to the system alignment and were calculated to be 48 degrees using a method posted by a designer of the King Snout objective.
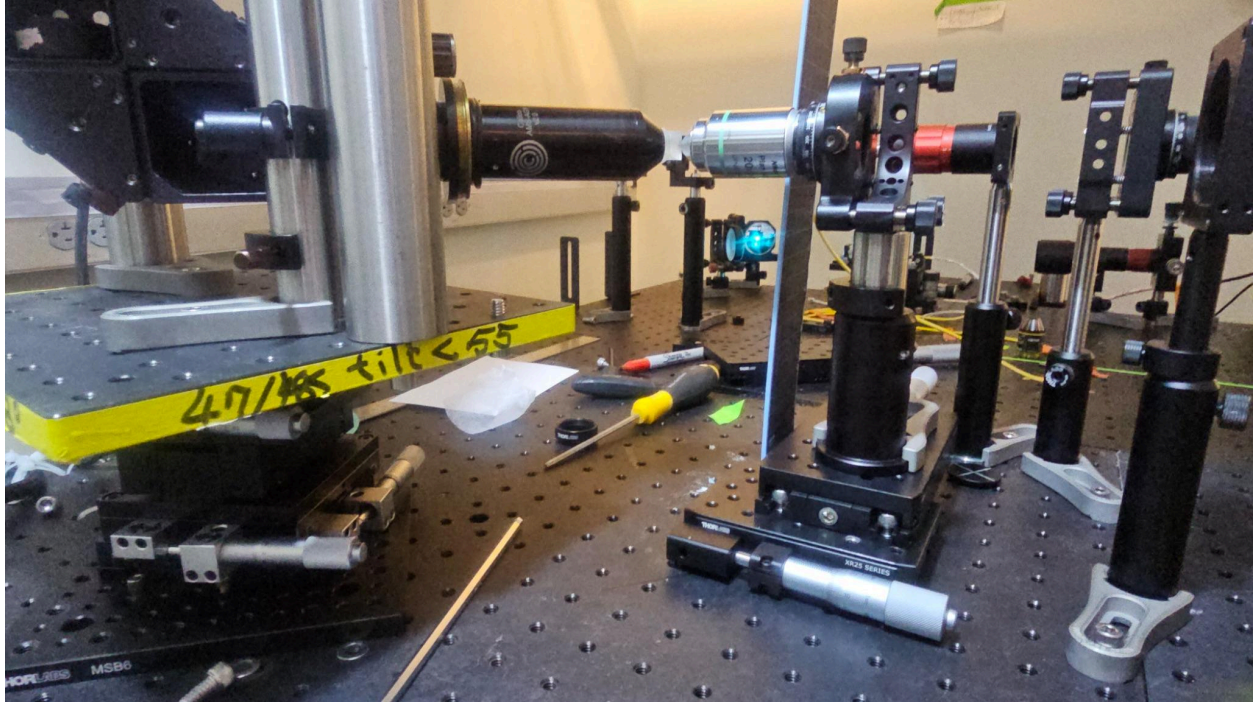
Figure 23. the alignment of the remote focusing and tertiary objectives

8. In addition to the improvements mentioned, we planned to upgrade the camera of our system. Previously, the system employed an Andor Zyla 4.2 PLUS SCMOS Camera, which achieved a frame rate of 100 fps at full frame (2048 x 2048 pixels). This setup allowed us to achieve a zebrafish volume rate of 3 to 4 Hz, which was not optimal for newer generations of genetically encoded calcium indicators (GECI) and genetically encoded voltage indicators (GEVI). Existing zebrafish whole-brain imaging studies, however, had even slower volume rates, barely reaching 0.8-3 Hz. The bottleneck of scanning speed imposed by the galvo-scanner was around 1 kHz at a small angle, indicating that a camera with a frame rate matched to this scanning speed would significantly boost the volumetric acquisition speed of SCAPE. Additionally, for voltage imaging, upgrading the galvo scanner may also be necessary.

Next, I outlined a timeline to finish up our system alignment in the next few weeks to enable biological data taking. It is important to note that further refinement may be needed depending on our imaging requirements. The task descriptions and estimated completion times are listed in Table 4.

Task Description	Projected Start and Completion Dates
fine tune the alignment of the system	May 17, 2024 - May 31, 2024
calibrate the system before biological imaging using beads and/or targets	May 20, 2024 - May 31, 2024
start data collection and update components as needed	June 1, 2024 and onwards

Table 4. Timeline for completion of our single objective lightsheet alignment

2.3.2 Dual Objective Light Sheet Microscope (DOLS)

We here optimized the translational mirror-based remote refocusing strategy [43,44,47,48] to enhance the volume scan rate of light-sheet microscopy. We chose a camera capable of balancing speed, noise, and resolution, and used it in a distributed planar imaging strategy configuration. With our microscope, we could capture voltage activity of neurons distributed across the brain of a larval zebrafish, at 200.8 Hz. Using a 5 day post fertilization (d.p.f.) zebrafish expressing Positron2-Kv, we found that we could image ~85% of the zebrafish brain, with the remainder either shadowed by the eye or scattering light. When two investigators hand-delineated the ROIs that corresponded to putative neurons, they identified 25,556 putative neurons, about 1/3 of the neurons of the zebrafish brain at that age.

We have identified missing frames (roughly 1 per every 2000 frames) while saving images from this microscope. This issue is likely due to the constrained memory of the acquisition computer and the slow write speed of the hard drives. Due to the large volume of the data and limited computer storage/memory , we were only able to record less than 1 minute time lapse of voltage imaging. To comprehensively record and integrate stimuli, neural activity, and behavioral aspects in our zebrafish study, we aim to establish a more reliable pipeline. This pipeline should have the capability to automatically transfer data to a robust analysis cluster like OpenMind or MIT's Engaging Cluster[60]. Such an upgrade would significantly enhance our data management and analysis efficiency.

This work is collaborated with Zeguan Wang, who built the majority of the optical setup for the Dual Objective Lightsheet Microscope and Jack Zhang who designed a customized camera board. I built sound stimulation chambers and setup, helped with fish preparation, dye, embedding, screening in some of the data taking, as well as tail tracking setup and microscope data taking and calibration. I am involved in building the data analysis pipeline that includes preprocessing, segmentation and other sections below.

2.4 Data processing and analysis

2.4.1 Pre-processing:

We first parsed the data stream from the camera into 30 videos corresponding to 30 z-stacks layers. Due to the high data throughput from the camera to the host computer through the PCIe bus (~2.6 GBps per camera), we identified roughly 1 dropped frame in every 2000 frames. To rectify a lost frame, we simply replaced it with linearly interpolated pixels data from the frames corresponding to adjacent layers immediately preceding and following it.

We first synchronized videos from the two cameras by time-aligning them at the light-sheet excitation laser onset at the beginning of the experiment. We then merged individual frames from the two cameras into a single frame for each time point. Each C-FOV captures approximately

half of the fish's brain from the midline to the left and right lateral sides . The combined frame size is 512 x 1280 pixels, with C-FOV encompassing the entire brain. Lastly, we concatenate corresponding z-stack frames from successive trials in time into a single video for motion correction, ROI segmentation, and temporal trace extraction.

2.4.2 ROI segmentation:

We extracted ROIs using manual labeling and automated ROI extraction methods. During the manual annotation process, we labeled two types of ROIs. Firstly, we identified and outlined objects that were approximately the size of a neuron (~9 pixels or 6.6 µm) and had ring-like boundaries. Secondly, for objects of a similar size to neurons, which we tentatively identified as neurons, we analyzed their temporal intensity traces. We then selected those objects whose intensity traces show narrow (<20ms), high amplitude, and positive-going spike signals. The annotated ROIs circled by Zeguan Wang were reviewed by me as shown in Figure 24. The percentage of ROIs that Zeguan Wang and I disagreed with was ~5% of all the annotated ROIs. The disagreement concentrated on the cases when there is no clear cell contour and examining the intensity traces of an object was needed. I aim to train the Volpy's Mask-RCNN[61] algorithm with our annotated dataset and additionally test and train other algorithms such as SegmentAnything[62] or cellpose 2.0 , as Volpy had difficulty segmenting our images in Figure 24.
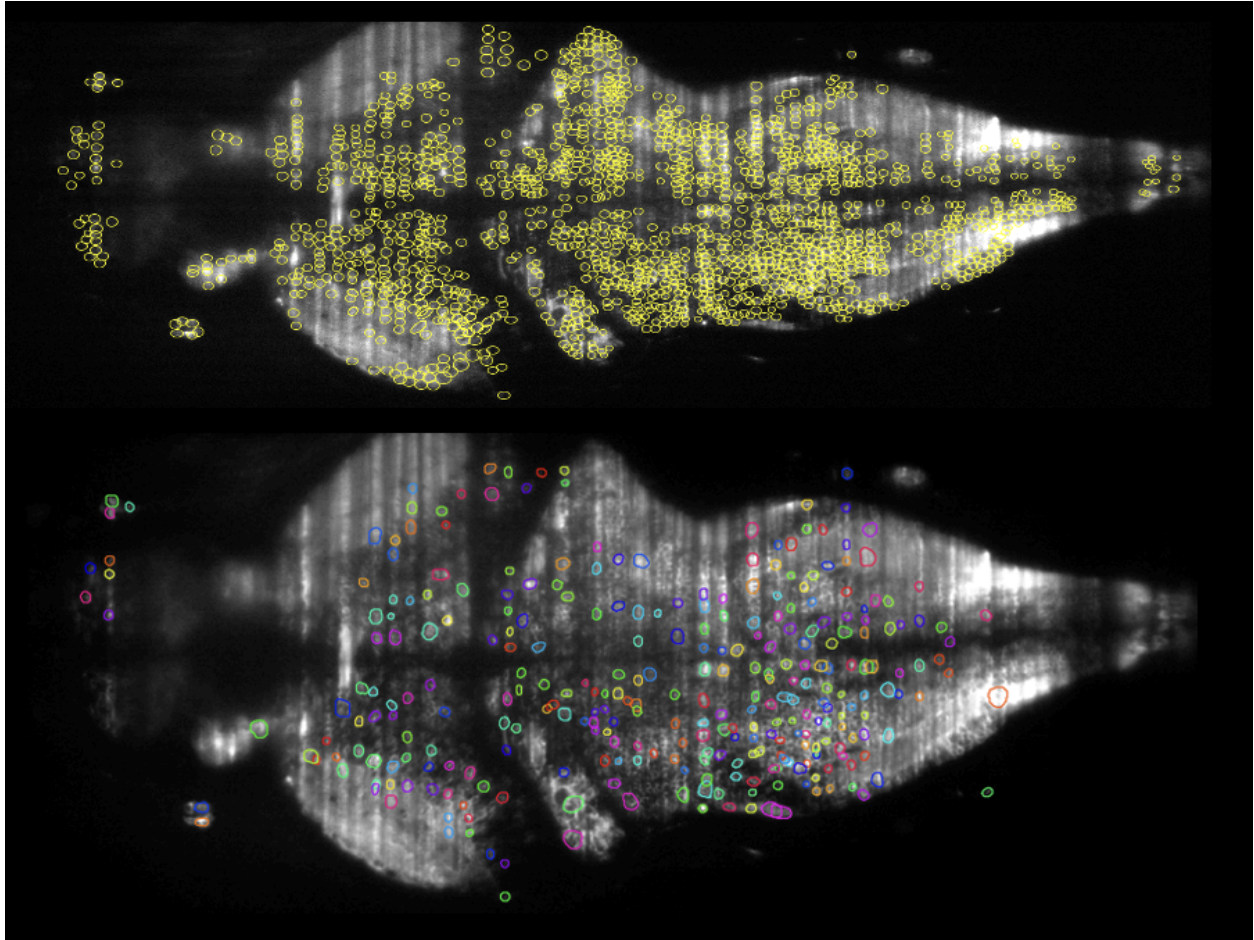
Figure 24. Hand annotated neurons and Volpy[63] annotated neuron comparison. The figure shows Volpy were not able to segment the ROI as accurately as manual annotation. This image was prepared in collaboration with Zeguan Wang and Jack Zhang

ROI temporal trace extraction: The extracted ROIs are processed by Volpy's temporal trace extraction pipeline, which is composed of background removal, trace denoising and spike extraction. After Volpy's pipeline[63], we further remove the ROIs with low SNR (<4) or ROIs with large overlap. The overlap is determined by calculating the spatial correlation between each ROI and all other ROIs. ROIs with over 0.9 correlation from existing ROIs are rejected as they are likely selecting the same cell.

The preprocessing and segmentation work was done in collaboration with Zeguan Wang, Jack Zhang and Panos Symvoudis. Zeguan and I collected some of the data together and I uploaded the data to the MIT openmind cluster. As it was sophisticated to sort data files coming from various stimuli and recording system and time consuming to sort/transfer data manually, I aim to build a more robust data acquisition and analysis pipeline that comprehensively record and integrate stimuli, neural activity, and behavioral data and automatically transfer data to an analysis cluster like OpenMind or MIT's Engaging Cluster.

I helped to align the images of the two cameras based on the code initially created by Jack Zhang and Ruihan Zhang. I submitted jobs to the openmind and engage cluster to help speed up the data processing process, and consulted MIT research computing to optimize the use of our group computational resources. I also helped to manually segment the region of interest and delineate traces using ImageJ. I am involved in testing and evaluating noise subtraction and motion artifact correction algorithms such as SUPPORT[64].

2.4.3 Behavior analysis:

Tail movements were concurrently monitored using IR illumination at approximately 200 frames per second (fps) via a substage optical path. Subsequently, tail coordinates and bending amplitude were analyzed utilizing a machine vision package known as Zebrazoom[65]. Figure 25 presented below showcases our behavioral recording imported into the Zebrazoom software. This powerful software enables the assessment of kinetic parameters of movement over time, notably the tail bending angle denoted by α. This angle is precisely defined as the angle between the body axis (depicted in pink) and the line connecting the core to the tip of the tail (illustrated in green). I plotted the tail bending angle across 5000 frames using ZebraZoom in the lower panel of Figure 25.

To summarize, we did not identify uniform behavior responses to our delivered sound stimuli across the population using our Positron2 line. More experiments and updates to the sound chamber are needed before drawing any conclusions. As described in the previous section, the

Positron2 fish exhibited certain behavior issues, leading us to suspect that they might have developmental issues impacting their auditory system. Another potential issue could be related to our sound delivery chamber. The fish were mounted to a plastic holder with agarose before being magnetically attached to the stimulation chamber, which might have affected sound propagation in the system.

Going forward, I plan to apply machine learning algorithms to systematically categorize these movement patterns, potentially identifying new behavioral types. I also want to leverage computer vision packages such as DeepLabCut[35], which support multi-point pose estimation, to explore intricate details of behaviors involving the fish's eyes, mouth, side fins, and tail, allowing for a finer level of analysis that was previously unattainable.
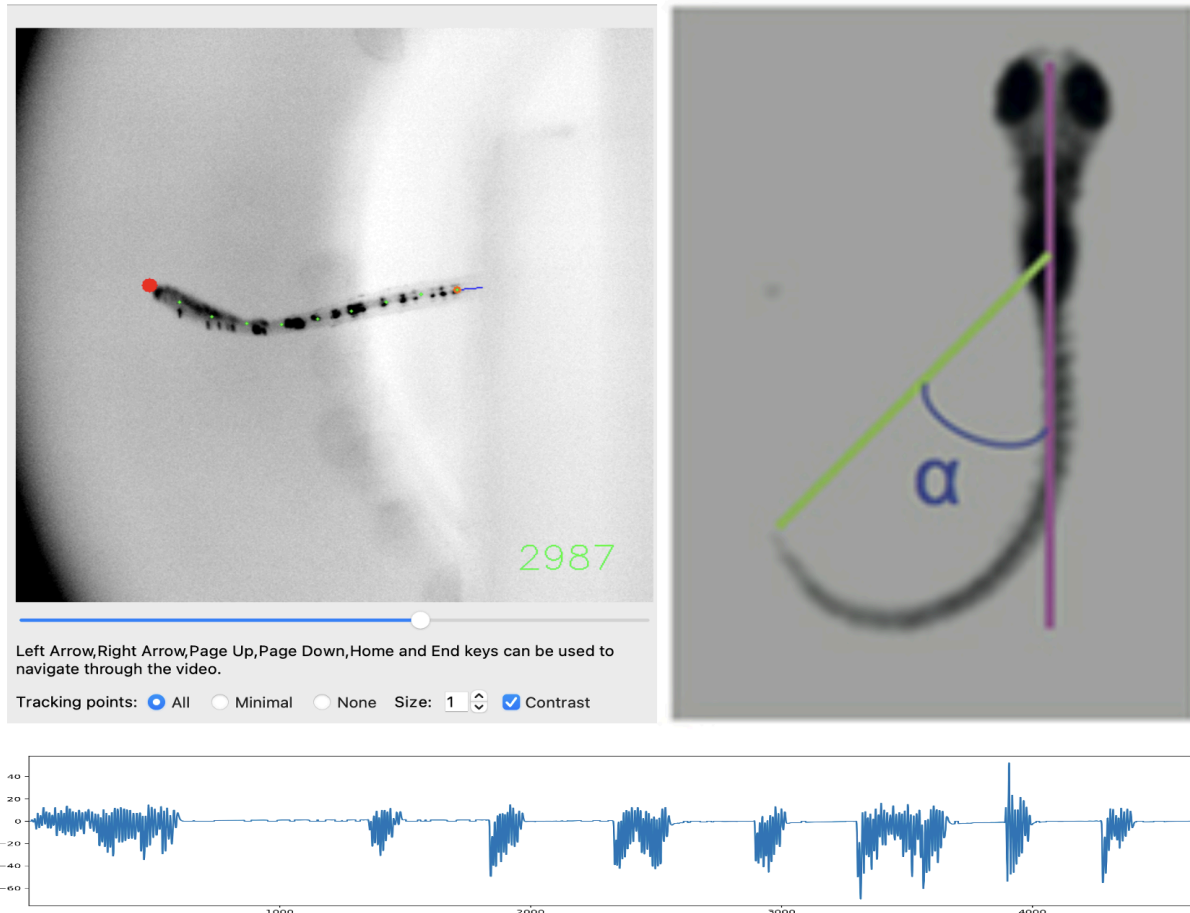
Figure 25. top left: behavioral recording imported into the Zebrazoom[66] software; top right: the tail bending angle denoted by α, defined as the angle between the body axis (depicted in pink) and the line connecting the core to the tip of the tail (illustrated in green); bottom: tail bending angle across 5000 frames produced with a Positron2 fish.

2.4.4 Image registration to ZBrain Atlas (on-going):

Z-Brain[17] atlas is a collective zebrafish neuron map contributed by multiple research groups. Registration to Z-Brain atlas would enable direct data set comparison among fish populations and help identifying robust biological patterns that offer more conclusive insights into neural functions. I am working on registering our functional dataset, obtained through the light-sheet

microscope in this study, to the comprehensive anatomical data in the Z-Brain atlas, based upon confocal microscopy. By imaging the same zebrafish using both techniques, we can align our specific data to the Z-Brain atlas. This alignment will facilitate the seamless correlation of anatomical locations between confocal and lightsheet coordinates, but also empower us to accurately identify anatomical regions of interest and allow screening for anatomically conserved neural clusters across fish populations.

2.4.5 Whole brain functional clustering (on-going):

This section is work in progress for my doctorate degree. The methodology based on the guidelines provided in the Ahrens paper[29] aims to delineate functional clusters of neurons in the zebrafish brain by combining activity-based clustering with regression analysis to identify neurons associated with specific sensory stimuli or motor movements. Adjustments and refinements may be necessary based on the experimental design and available data:

First, we can cluster neurons based on their activity patterns and correlations. Apply clustering algorithms (such as k-means, hierarchical clustering, or spectral clustering) to group neurons exhibiting similar activity patterns.

Second, we can then perform regression analysis to correlate neural activity with specific stimuli (visual, olfactory) or motor movements. Calculate regression coefficients of ROIs to sensory stimuli or motor movement regressors to identify functional neurons associated with these stimuli or movements.

Third, we can conduct sub-component analysis and tune our focus to particular functional components, such as motor neurons. We can distinguish between spontaneous motor activity and stimulus-driven motor activity and identify motor neurons exhibiting either or both features by plotting regression coefficients against corresponding regressors.

Fourth, we can validate our findings by comparing them across fish populations, and with existing knowledge or experimental paradigms while registering our dataset to ZBrain Atlas.

2.4.6 Future Work: Network dynamics and behavior modeling/prediction:

Inspired by Florian Engert's work on an integrator model incorporating decision thresholds for visual reflexes [67,68], our aim is to broaden this framework's scope to encompass non-reflexive behavior classifications triggered by stimuli such as olfaction and sound. Our future trajectory involves developing an extensive model that not only replicates single-episode decision-making but also encapsulates sensory integration and sequential behavior patterns across varying time sequences. This endeavor will leverage insights from Reinforcement Learning, Markov Decision Processes (MDPs), and other pertinent frameworks. The modeling of network dynamics not only holds promise in understanding zebrafish behavior but also stands to provide valuable feedback for constructing more robust and efficient AI algorithms that mirror real-life biological cognition and decision-making processes.

Chapter 3: Conclusions and Discussions

Whole brain imaging in small entire brains can have profound implications across numerous fields including medicine [69,70], disease mechanism elucidation [69, 71], and artificial intelligence[72]. The capacity to visualize the entire brain's activity in vivo allows researchers to observe neural interactions and behaviors in unprecedented detail, offering insights that are critical for understanding complex biological processes. The exploration of whole brain dynamics through imaging technologies like voltage and calcium imaging has opened new avenues for research. Voltage imaging provides real-time monitoring of electrical activities across neurons, offering a direct measure of brain function. Calcium imaging, on the other hand, tracks calcium ions within neurons, a proxy for neural activity. Each method has its advantages and particular uses, depending on the resolution and temporal dynamics required for specific research questions. We still need to work on optimizing a voltage zebrafish line for whole brain imaging and keep making improvements in microscopy hardware attempting to reveal zebrafish whole brain dynamics at ground truth level.

Significant technical enhancements have been necessary to optimize the SCAPE 2.0 to match our desired field of view, resolution, and ease of alignment. These modifications are crucial for capturing high-quality images that are both detailed and comprehensive. Moving forward, careful consideration is essential before making a decision to adopt published microscope design v.s. designing and building a system of our own. As I continue my PhD studies, I am committed to advancing these technologies and methodologies, as well as delving deeper into data analysis and modeling. The ability to image whole brain dynamics holds vast potential not only for neuroscience but also for informing the development of artificial intelligence models. By understanding how a smaller, simpler brain processes information and adapts, we can derive principles applicable to AI algorithms, potentially leading to more robust and adaptive artificial systems. There remains much work to be done on improving fishline genetics, enhancing imaging systems, and developing more sophisticated data analysis techniques and I look forward to tackling these challenges over the course of my PhD journey.

Ethical Responsibilities

All animal protocols were approved by the Committee on Animal Care (CAC), an Institutional Animal Care and Use Committee (IACUC) responsible for overseeing animal research. As of now, there are no anticipated ethical concerns associated with these animal experiments. However, looking ahead, in the event that we can successfully simulate and predict the neural and behavioral responses of various animals (e.g., worms, fish, mice, or humans) when presented with specific stimuli, there arises the potential for misuse, including manipulation and control without the subject's consent. To mitigate these risks, it is imperative to establish a robust regulatory framework aimed at safeguarding against ethical abuses. Researchers must strike a delicate balance between scientific progress, technological advancement, and ethical responsibility to ensure that advancements are made ethically and with proper consideration for potential societal implications.

References

1. Mendl, M. & Paul, E. S. Animal affect and decision-making. *Neurosci. Biobehav. Rev.* **112**, 144–163 (2020).

2. Davidson, H. G., Scherer, K. & Goldsmith, H. H. Handbook of affective science (pp. 619-642). Preprint at (2007).

3. Tinbergen, N. On aims and methods of Ethology. *Z. Tierpsychol.* **20**, 410–433 (2010).

4. Marr, D. *Vision: A Computational Investigation into the Human Representation and Processing of Visual Information*. (MIT Press, 2010).

5. Durairaj, B. & Dhanabal, M. Zebrafish as a prodigious tool in neuropsychiatric research. *The Journal of Basic and Applied Zoology* **81**, 1–6 (2020).

6. JGCaMP8 calcium indicators. *Janelia Research Campus* https://www.janelia.org/node/65790.

7. Zhang, Y. *et al.* Fast and sensitive GCaMP calcium indicators for imaging neural populations. *Nature* **615**, 884–891 (2023).

8. Shemesh, O. A. *et al.* Precision Calcium Imaging of Dense Neural Populations via a Cell-Body-Targeted Calcium Indicator. *Neuron* **107**, 470–486.e11 (2020).

9. Villette, V. *et al.* Ultrafast Two-Photon Imaging of a High-Gain Voltage Indicator in Awake Behaving Mice. *Cell* **179**, 1590–1608.e23 (2019).

10. Abdelfattah, A. S. *et al.* Sensitivity optimization of a rhodopsin-based fluorescent voltage indicator. *Neuron* **111**, 1547–1563.e9 (2023).

11. Kannan, M. *et al.* Dual-polarity voltage imaging of the concurrent dynamics of multiple neuron types. *Science* **378**, eabm8797 (2022).

12. Voltron and positron. *Janelia Research Campus* https://www.janelia.org/open-science/voltron-and-positron.

13. Kawakami, K. Transposon tools and methods in zebrafish. *Dev. Dyn.* **234**, 244–254 (2005).

14. Abdelfattah, A. S. *et al.* A general approach to engineer positive-going eFRET voltage indicators. *Nat. Commun.* **11**, 3444 (2020).

15. Abdelfattah, A. S. *et al.* Bright and photostable chemigenetic indicators for extended in vivo voltage imaging. *Science* **365**, 699–704 (2019).

16. Randlett, O. *et al.* Whole-brain activity mapping onto a zebrafish brain atlas. *Nat. Methods* **12**, 1039–1046 (2015).

17. Z Brain Atlas. https://zebrafishexplorer.zib.de/home/.

18. Yang, J. *et al.* Solaris: a panel of bright and sensitive hybrid voltage indicators for imaging membrane potential in cultured neurons. *bioRxiv* 2024.02.02.578569 (2024) doi:10.1101/2024.02.02.578569.

19. Kermen, F., Franco, L. M., Wyatt, C. & Yaksi, E. Neural circuits mediating olfactory-driven behavior in fish. *Front. Neural Circuits* **7**, 62 (2013).

20. Herrera, K. J., Panier, T., Guggiana-Nilo, D. & Engert, F. Larval Zebrafish Use Olfactory Detection of Sodium and Chloride to Avoid Salt Water. *Curr. Biol.* **31**, 782–793.e3 (2021).

21. Jeong, Y.-M. *et al.* Optogenetic Manipulation of Olfactory Responses in Transgenic Zebrafish: A Neurobiological and Behavioral Study. *Int. J. Mol. Sci.* **22**, (2021).

22. Braubach, O. R., Wood, H.-D., Gadbois, S., Fine, A. & Croll, R. P. Olfactory conditioning in the zebrafish (Danio rerio). *Behav. Brain Res.* **198**, 190–198 (2009).

23. Poulsen, R. E. *et al.* Broad frequency sensitivity and complex neural coding in the larval zebrafish auditory system. *Curr. Biol.* **31**, 1977–1987.e4 (2021).

24. A profile of auditory‑responsive neurons in the larval zebrafish brain.

25. Privat, M. *et al.* Sensorimotor Transformations in the Zebrafish Auditory System. *Curr. Biol.* **29**, 4010–4023.e4 (2019).

26. Bhandiwad, A. A., Zeddies, D. G., Raible, D. W., Rubel, E. W. & Sisneros, J. A. Auditory sensitivity of larval zebrafish (Danio rerio) measured using a behavioral prepulse inhibition assay. *J. Exp. Biol.*

216, 3504–3513 (2013).

27. Yang, Q., Sun, P., Chen, S., Li, H. & Chen, F. Behavioral methods for the functional assessment of hair cells in zebrafish. *Front. Med.* 11, 178–190 (2017).

28. Circuit mechanisms for colour vision in zebrafish.

29. Chen, X. *et al.* Brain-wide Organization of Neuronal Activity and Convergent Sensorimotor Transformations in Larval Zebrafish. *Neuron* 100, 876–890.e5 (2018).

30. Bollmann, J. H. The Zebrafish Visual System: From Circuits to Behavior. *Annu Rev Vis Sci* 5, 269–293 (2019).

31. Sy, S. K. H. *et al.* An optofluidic platform for interrogating chemosensory behavior and brainwide neural representation in larval zebrafish. *Nat. Commun.* 14, 227 (2023).

32. Candelier, R. *et al.* A microfluidic device to study neuronal and motor responses to acute chemical stimuli in zebrafish. *Sci. Rep.* 5, 12196 (2015).

33. BATS. https://be.mit.edu/news-events/bats/2074.

34. Han, X. *et al.* A polymer index-matched to water enables diverse applications in fluorescence microscopy. *Lab Chip* 21, 1549–1562 (2021).

35. Mathis, A. *et al.* DeepLabCut: markerless pose estimation of user-defined body parts with deep learning. *Nat. Neurosci.* 21, 1281–1289 (2018).

36. Green, M. H., Ho, R. K. & Hale, M. E. Movement and function of the pectoral fins of the larval zebrafish (Danio rerio) during slow swimming. *J. Exp. Biol.* 214, 3111–3123 (2011).

37. Hillman, E. M. C., Voleti, V., Li, W. & Yu, H. Light-Sheet Microscopy in Neuroscience. *Annu. Rev. Neurosci.* 42, 295–313 (2019).

38. Stelzer, E. H. K. *et al.* Light sheet fluorescence microscopy. *Nature Reviews Methods Primers* 1, 1–25 (2021).

39. Corsetti, S., Gunn-Moore, F. & Dholakia, K. Light sheet fluorescence microscopy for neuroscience. *J. Neurosci. Methods* 319, 16–27 (2019).

40. Power, R. M. & Huisken, J. A guide to light-sheet fluorescence microscopy for multiscale imaging. *Nat. Methods* **14**, 360–373 (2017).

41. Ahrens, M. B., Orger, M. B., Robson, D. N., Li, J. M. & Keller, P. J. Whole-brain functional imaging at cellular resolution using light-sheet microscopy. *Nat. Methods* **10**, 413–420 (2013).

42. Vladimirov, N. *et al.* Light-sheet functional imaging in fictively behaving zebrafish. *Nat. Methods* **11**, 883–884 (2014).

43. Botcherby, E. J., Juskaitis, R., Booth, M. J. & Wilson, T. Aberration-free optical refocusing in high numerical aperture microscopy. *Opt. Lett.* **32**, 2007–2009 (2007).

44. Botcherby, E. J., Juškaitis, R., Booth, M. J. & Wilson, T. An optical technique for remote focusing in microscopy. *Opt. Commun.* **281**, 880–887 (2008).

45. Creators Alfred Millett-Sikking1 Nathaniel H. Thayer2 Adam Bohnert2 Andrew G. York2 Show affiliations 1. @Calico 2. @calico. *Calico/remote_refocus: Pre-Print*. doi:10.5281/zenodo.1146084.

46. Fahrbach, F. O., Voigt, F. F., Schmid, B., Helmchen, F. & Huisken, J. Rapid 3D light-sheet microscopy with a tunable lens. *Opt. Express* **21**, 21010–21026 (2013).

47. Sparks, H. *et al.* Development a flexible light-sheet fluorescence microscope for high-speed 3D imaging of calcium dynamics and 3D imaging of cellular microstructure. *J. Biophotonics* **13**, e201960239 (2020).

48. Dibaji, H. *et al.* Axial de-scanning using remote focusing in the detection arm of light-sheet microscopy. *Res Sq* (2023) doi:10.21203/rs.3.rs-3338831/v1.

49. Yang, B. *et al.* Epi-illumination SPIM for volumetric imaging with high spatial-temporal resolution. *Nat. Methods* **16**, 501–504 (2019).

50. Yang, B. *et al.* DaXi-high-resolution, large imaging volume and multi-view single-objective light-sheet microscopy. *Nat. Methods* **19**, 461–469 (2022).

51. Sapoznik, E. *et al.* A versatile oblique plane microscope for large-scale and high-resolution imaging of subcellular dynamics. *Elife* **9**, (2020).

52. Hoffmann, M. & Judkewitz, B. Diffractive oblique plane microscopy. *Optica* **6**, 1166 (2019).

53. Hoffmann, M., Henninger, J., Richter, L. & Judkewitz, B. Brain-wide imaging of an adult vertebrate with image transfer oblique plane microscopy. *bioRxiv* 2022.05.16.492103 (2022) doi:10.1101/2022.05.16.492103.

54. Kumar, M., Kishore, S., Nasenbeny, J., McLean, D. L. & Kozorovitskiy, Y. Integrated one- and two-photon scanned oblique plane illumination (SOPi) microscopy for rapid volumetric imaging. *Opt. Express* **26**, 13027–13041 (2018).

55. Voleti, V. *et al.* Real-time volumetric microscopy of in vivo dynamics and large-scale samples with SCAPE 2.0. *Nat. Methods* **16**, 1054–1062 (2019).

56. Bouchard, M. B. *et al.* Swept confocally-aligned planar excitation (SCAPE) microscopy for high speed volumetric imaging of behaving organisms. *Nat. Photonics* **9**, 113–119 (2015).

57. Daniels, J. Help us make King Snout a reality. *ASI | Applied Scientific Instrumentation* https://www.asiimaging.com/frontpage-article/blog/help-us-make-king-snout-a-reality/ (2020).

58. Yang, B. *et al.* High-Resolution, Large Imaging Volume, and Multi-View Single Objective Light-Sheet Microscopy. *bioRxiv* 2020.09.22.309229 (2021) doi:10.1101/2020.09.22.309229.

59. AdlOptica πShaper Flat Top Beam Shapers. https://www.edmundoptics.com/f/flat-top-beam-shapers/15036/.

60. MIT campus-wide resources. https://orcd.mit.edu/resources/mit-campus-wide-resources.

61. *Mask_RCNN: Mask R-CNN for Object Detection and Instance Segmentation on Keras and TensorFlow*. (Github).

62. Segment anything. https://segment-anything.com.

63. Cai, C. *et al.* VolPy: Automated and scalable analysis pipelines for voltage imaging datasets. *PLoS Comput. Biol.* **17**, e1008806 (2021).

64. Eom, M. *et al.* Statistically unbiased prediction enables accurate denoising of voltage imaging data. *Nat. Methods* **20**, 1581–1592 (2023).

65. ZebraZoom. http://Zebrazoom.org.

66. Mirat, O., Sternberg, J. R., Severi, K. E. & Wyart, C. ZebraZoom: an automated program for high-throughput behavioral analysis and categorization. *Front. Neural Circuits* **7**, 107 (2013).

67. Bahl, A. & Engert, F. Neural circuits for evidence accumulation and decision making in larval zebrafish. *Nat. Neurosci.* **23**, 94–102 (2020).

68. Larval zebrafish as a model for perceptual decision-making. https://www.hfsp.org/hfsp-news/larval-zebrafish-model-perceptual-decision-making.

69. Duque, M. *et al.* Ketamine modulates a norepinephrine-astroglial circuit to persistently suppress futility-induced passivity. *bioRxiv* 2022.12.29.522099 (2023) doi:10.1101/2022.12.29.522099.

70. Kalueff, A. V., Stewart, A. M. & Gerlai, R. Zebrafish as an emerging model for studying complex brain disorders. *Trends Pharmacol. Sci.* **35**, 63–75 (2014).

71. Thyme, S. B. *et al.* Phenotypic Landscape of Schizophrenia-Associated Genes Defines Candidates and Their Shared Functions. *Cell* **177**, 478–491.e20 (2019).

72. Pan, W., Zhao, F., Han, B., Dong, Y. & Zeng, Y. Emergence of brain-inspired small-world spiking neural network through neuroevolution. *iScience* **27**, 108845 (2024).